LightVest

A smart vest to provide visible light communication inside pockets

by

Jard Wesdorp

Supervisor: Dr. Marco Antonio Zuniga Zamalloa
Faculty: Networked Systems group, TU Delft

TU Delft

LightVest

A smart vest to provide visible light communication inside pockets

by

Jard Wesdorp

to obtain the degree of Master of Science
at the Delft University of Technology,
to be defended publicly on Tuesday September 10, 2024 at 16:00 PM.

Project duration:	November 20, 2023 – September 10, 2024	
Thesis committee:	Dr. R. Venkatesha Prasad	TU Delft,
	Prof. dr. K. G. Langendoen	TU Delft,
	Dr. M. A. Zúñiga Zamalloa	TU Delft,

An electronic version of this thesis is available at `http://repository.tudelft.nl/`.

TU Delft

Preface

Already in my bachelor's, I was fascinated by embedded systems. After my embedded systems minor, I wanted to continue this fascination by doing a master's at TU Delft. During this time, I learned a lot. In the last quarter of the first year, I followed the course "Visible Light Communication and Sensing", which I found very interesting. So I contacted Marco Zuniga to see if I could do a thesis with him.

I would like to thank my girlfriend and friends for supporting me, and I want to especially thank Marco Zuniga for the valuable supervision, feedback and guidance during my thesis. I am excited to work with him to further progress this thesis into a paper and help him with another interesting project.

Jard Wesdorp
Delft, September 2024

Abstract

Visible light communication (VLC) has gained attention recently as radio frequencies become increasingly congested. VLC offers a promising alternative for wireless communication with several advantages: It provides 10 times more bandwidth than traditional radio frequencies, is more energy-efficient and secure, and can take advantage of the existing lighting infrastructure. However, VLC also has drawbacks, such as its susceptibility to ambient light interference and its dependence on a clear line of sight (LOS). When the receiver is obstructed, such as being placed in a pocket, the signal is blocked, and communication fails.

We address one of the most important NLOS scenarios in VLC: when users place the receiver inside the pocket. Our system places photodiodes on a 3D-printed vest to capture the optical data and then forwards the information to the phone inside the pocket using near-field communication (NFC).

We introduce several optimizations to enhance the performance of LightVest. First, we develop a novel method for optimizing photodiode placement on the vest using the Lambertian propagation model, ensuring optimal angles for maximum signal reception. Additionally, we implement adaptive filtering and threshold techniques to maintain reliable communication in dynamic environments, improving the VLC system's robustness against noise and movement. We also optimize the software to increase the sampling rate, reducing processing times. These improvements result in a maximum data rate of 25 kbps and a range of 220 cm at a data rate of 5 kbps with a bit error rate of 0.025.

We enhanced the NFC link using techniques like Fast Transfer Mode and non-blocking I2C to achieve a maximum data rate of 21 kbps. To facilitate user interaction with the LightVest, we developed an Android application to control the microcontroller. In addition, it provides data visualization and collection, significantly speeding up the debugging and experimentation processes.

Overall, LightVest represents an advancement in extreme NLOS and wearable VLC, paving the way for future innovations in secure and wearable VLC solutions. Future work could focus on improving the performance of the VLC link by selecting a more powerful microcontroller, using enhanced filtering, and adopting a more advanced modulation scheme. Future efforts could also include adding an uplink to the system to complete the VLC setup and exploring alternative vest designs by using a vest or shirt instead of a 3D model.

Contents

1

Introduction

1.1. Introduction

Visible light communication (VLC) is a relatively new and upcoming wireless communication technique. It uses visible light to communicate data wirelessly. A "spectrum deficit" in radio frequencies, especially Wi-Fi, was expected because of the exponential growth of demand for wireless devices [18]. Because of this, alternatives need to be researched to have reliable wireless communication in the future.

VLC can be a good alternative because of its many positive properties. It has 10x more bandwidth compared to radio frequencies, from 430 MHz to 77 THz, more efficient energy consumption, more security, no electromagnetic interference, and is not affected by Wi-Fi or cellular technologies (4G/5G/6G). Furthermore, it can take advantage of the existing infrastructure, such as LED lighting, making it a cost-effective solution.

However, VLC also has challenges. Issues such as light dimming, flickering, and the system's susceptibility to ambient light noise can decrease its performance. Additionally, VLC's reliance on a clear line of sight (LOS) between the transmitter and receiver is a significant limitation. When the LOS is obstructed, whether by the environment or by something simple like a human body, communication becomes very limited or non-existent. Examples of this are illustrated in figure 1.1.

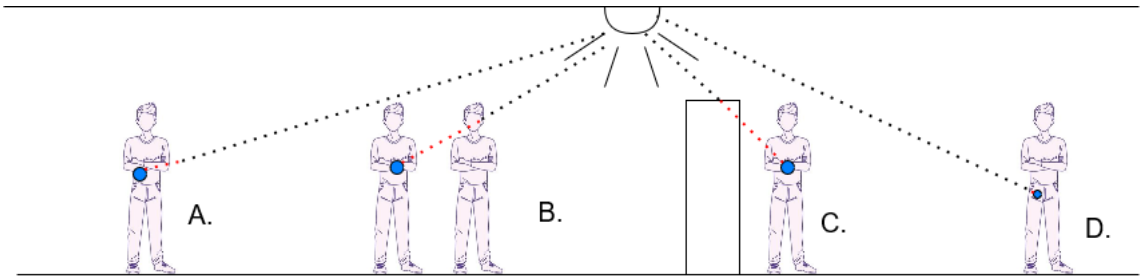

Figure 1.1: NLOS in VLC: A: the body of the person blocks the LOS, B: Another person blocks the LOS, C: A structure blocks the LOS, D: NLOS because the receiver is inside the pocket

Some papers have tried to find solutions for this problem, such as Cui et at., where they used the side RF-channel created by the VLC [11]. Thus, they could still receive the data while the LOS is blocked. However, this solution would not work if the transmitter is protected with electrical shielding. Beyens et al. tried to solve the non-LOS problem by guiding users towards a direction where they obtain an optimal VLC link, this is a good solution, but it needs a user-in-the-loop system [5].

However, none of these papers consider the problem that arises when users put the receiver in a pocket. This thesis focuses on finding a solution to this extreme NLOS problem.

1.2. Research questions

The main problem we want to solve is when VLC is ineffective because the receiver is in a pocket. The main research question for this thesis is:

How to receive Visible Light Communication while having the receiver inside a pocket?

Besides the main research question, there are other sub-research questions:

1. How can we design a solution to this problem?
2. Where do you place the receivers?
3. How do you design an efficient link?
4. How does the solution perform in a practical environment?

1.3. Contributions

The solution presented in this thesis is **LightVest**, a system that can streamline the data sent with VLC to a phone while inside a pocket. This is achieved by using photodiodes placed strategically on a 3D-printed vest to receive the data. A microcontroller then processes and transmits the data to the phone using NFC. In figure 1.2 LightVest is visualized.

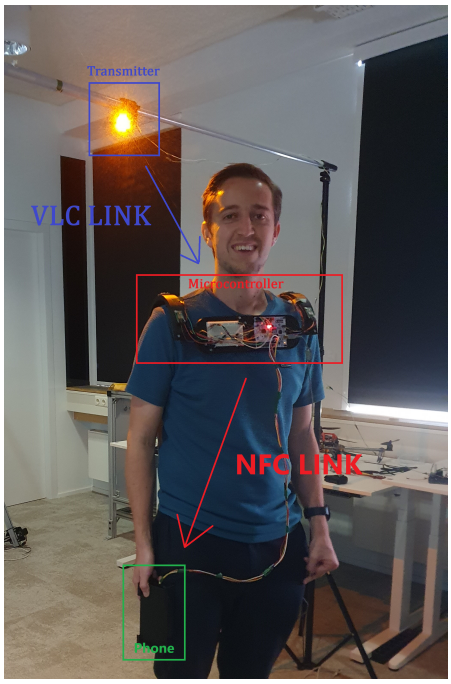

Figure 1.2: LightVest with its main components, including VLC link, NFC link, and a Android system with an app installed.

The LightVest consists of three main components: a VLC Link, an NFC link, and an Android App.

VLC Link
We apply multiple measures to find the optimal link. First, we use the Lambertian propagation model to determine the best-performing angles of the photodiodes. Then, we optimize the link performance with multiple techniques, such as filtering, adaptive and resetting threshold, and the MCU performance is improved to reach a maximum sampling rate of 544 kHz.

NFC Link
For the NFC link, we improve the communication link by using Fast Transfer Mode, implementing a non-blocking I2C, and buffering the received messages.

Android System
Regarding the Android system, we have developed an application that can be installed on an Android phone. With this Android App, LightVest can be controlled, speeding up the debugging process for improving the VLC link and retrieving experiment results.

1.4. Environments

The LightVest has the potential to be used in a variety of indoor environments. For example, in settings where the lighting infrastructure is already set up, it can be used as a transmitter for the system as the downlink.

One important property of VLC is its inherent privacy. Light cannot penetrate walls, making VLC an ideal option for environments that require secure wireless communication. This is particularly beneficial in sensitive labs or military locations, where data security is important.

The LightVest is also useful to people who already have to wear work clothes, some examples can be seen in figure 1.3. These clothing are already equipped with pockets for their phones, so an NFC antenna could be placed behind the pocket to enable an NFC connection.

Figure 1.3: Examples for clothing with phone holders

2 Background

In this chapter, we provide background information about VLC to understand the choices we made when implementing the NFC link.

2.1. VLC Transmitter

The transmitter in the VLC system modulates light to transmit information. We delve into different transmitters, such as light-emitting diodes, screens, and passive light sources such as ambient light.

2.1.1. Light Emitting Diode

The most common type of transmitter in VLC is a Light-Emitting Diode (LED). LEDs are preferred due to their ability to switch on and off at very high speeds, which is essential for fast data transmission. There are multiple different kinds of LEDs, examples are Phosphor converted LEDs, Multi-Chip LEDs, organic LEDs and Micro-LEDs [26]. Each has its unique properties and advantages. LEDs are widely used in general lighting, which makes them a practical and cost-effective choice.

RGB LEDs are also frequently used in VLC systems. By modulating information across different colours, they can transmit data through separate channels, increasing the data rate and enabling more complex communication schemes.

2.1.2. Screens

Screens are another alternative for a VLC transmitter. They can transmit data by encoding data into the screen's pixels while making it invisible to the human eye [35, 23]. This technique can have a high data rate, but it is often prone to noise and does not have a long range.

2.1.3. Passive light

Some research is done using passive light as a source for the VLC transmitter [36, 16]. Using sunlight, those studies transmit data by modulating the polarization of the light. While this method is innovative, it is still in the early stages of development and does not support high data rates.

In this thesis, we focus on using the existing lightning structure. Thus, LED is used as the transmitter for our VLC system.

2.2. VLC Receiver

The receiver in a VLC system is a crucial component responsible for capturing the transmitted light and converting it into an electrical signal for further processing. Various types of receivers can be employed, each with advantages and limitations.

2.2.1. Photodiode
A photodiode is one of the most commonly used receivers in VLC systems. It produces an electric current when absorbing photon radiation, such as visible light or infrared. Due to its fast response time, the photodiode is highly suitable for high-speed data communication applications, making it a preferred choice in VLC systems [26]. The output signal can be retrieved using an Analogue-to-Digital Converter (ADC) which can be further processed with a microcontroller or Field-Programmable Gate Array (FPGA) to obtain the information being sent.

2.2.2. Camera
A camera can also function as a receiver by capturing frames of transmitted light. These frames can be decoded using different methods to retrieve the transmitted data. However, the use of cameras as receivers is limited by their relatively low response time, primarily due to the low frame rates that cameras typically operate at. Additionally, the large amount of data that is generated requires significant processing power. This can lead to high power consumption compared to photodiodes. Despite that, they have the advantage of high spectral efficiency.

2.2.3. Alternative receivers
Research is also done into alternative receivers, such as solar panels [25] or an LED [17]. These options are not viable for us because of their high complexity and low response times.

Ultimately, we will use photodiodes in this thesis because of their high bandwidth and small size, this ensures that they can be placed on a vest without being too visible.

2.3. Modulation
Modulation is the process of encoding information in a transmitted signal. In the context of VLC, several types of modulations are possible. They can be differentiated into several types of modulation such as amplitude-based, pulse-based, colour-based, and complex-based [2]. However, two key issues must be addressed, dimming and flickering. Dimming occurs when the average intensity of light decreases due to modulation. During the modulation phase, there are periods when the light is off, causing a dimming effect. Flickering occurs when the frequency of the light is too low, causing visible fluctuations in brightness.

2.3.1. Amplitude base modulation
Amplitude-based modulation is the least complex modulation with On-Off-Keying (OOK) being the simplest since it only differentiates between binary states (1 and 0).

More advanced Amplitude-based modulations benefit from a higher spectral efficiency, such as Pulse Amplitude modulation (PAM)m where each pulse can represent multiple bits depending on the number of amplitude levels. Another example is Amplitude Shift Keying (ASK), here the data is encoded by the amplitude of the carrier wave. The downside of these modulations is that they need more complex designs.

2.3.2. Pulse modulation
Pulse modulation is encoded based on the timing and/or the width of pulses. Examples of pulse modulation are Pulse Width Modulation (PWM), Pulse Position Modulation (PPM), Variable Pulse Position Modulation (VPPM), Overlapping Pulse Position Modulation (OPPM), and Multi Pulse Position Modulation (MPPM) [2].

A more complex pulse modulation, Adaptive Multiple Pulse Position Modulation (AMPPM), has been explored by Wu et al. [38]. They implemented a modulation that avoids flickering while maximizing throughput under particular dimming levels.

Pulse modulation schemes are useful for environments where consistent light intensity (to avoid dimming) is crucial. However, they often require more advanced processing capabilities.

2.3.3. Colour shift keying

Colour Shift Keying (CSK) is a modulation technique that uses RGB LEDs to encode the signal. By varying the colour of the LED, data can be transmitted without interference, as each colour channel operates independently [27]. This modulation requires a multi-colour LED setup and a receiver capable of detecting the different colours.

2.3.4. Complex based modulation

Complex-based modulation techniques achieve high data rates because of their high spectral efficiency. Examples include Orthogonal Frequency Division Multiplexing (OFDM) [37] and Quadrature amplitude modulation (QAM) [20]. However, these techniques require complex hardware, powerful processors and sensitive receivers. They are also more susceptible to noise and interference, making them less robust. Due to their complexity and cost, these modulation schemes are typically reserved for scenarios where maximizing data throughput and efficiency is essential.

Since our goal in this thesis is not to maximize data rate, we implement OOK modulation with Manchester encoding because of its simplicity. The Manchester encoding is added to maintain the duty cycle of 50% to avoid flickering. However, this will cause the LED to have a dimming level of 50%.

Now that the basics of VLC have been introduced, we can examine its advantages and disadvantages.

2.4. Advantages and disadvantages

VLC has its advantages and disadvantages. but the advantages mostly outweigh the disadvantages. The advantages of VLC are:

1. **Existing infrastructure:** Many houses, offices or warehouses are already equipped with LED lighting. VLC can leverage this existing lighting infrastructure to implement a VLC system, making the buildings more energy-efficient and inherently less costly [8].
2. **High bandwidth:** VLC has a bandwidth of 390 THz [26], which is 10x times higher than Wi-Fi. Because of this, VLC can achieve higher data rates and more bandwidth to spread communication among each other.
3. **Electromagnetic interference** Since VLC does not create any electromagnetic interference, it can be safely used in medical environments where procedures are sensitive to electromagnetic waves. For example, paper [1] created a wearable patient monitoring device to safely extract information about the patient without creating sensitive electromagnetic waves.
4. **Security:** Inherently, VLC offers security because light cannot penetrate walls. This makes it difficult for intruders to eavesdrop on the data that is being sent. Some studies have tried to debunk this by eavesdropping using keyholes, gaps under the door, and windows [9]. These vulnerabilities can be mitigated by closing keyholes, sealing door gaps, and covering windows. Cui et al. [11] were able to eavesdrop using the side RF channel created by the switching LED's.

Unfortunately, there are also some properties which make VLC less desirable.

1. **Limited range:** One significant limitation is the range. Because communication travels through light, it has a restricted range, particularly when high data rates need to be achieved. This can limit its effectiveness for large-scale deployments where extensive coverage is required.
2. **Ambient light:** The effect of ambient light such as sunlight or light from non-VLC light sources can cause interference on VLC, degrading the communication quality and reliability. A reliable connection can be challenging to maintain in environments with variable lighting conditions.
3. **Line-of-sight** VLC typically requires a line of sight between transmitter and receiver. Obstacles like walls, furniture, people, or even pockets can obstruct the light path, disrupting communication.
4. **Mobility** Maintaining a reliable connection during the movement of either the transmitter or receiver can be difficult due to fluctuations in the signal. This makes VLC less suitable for applications involving high mobility, such as in vehicles or for mobile devices in active use.

Designing a practical solution to the problem of having the receiver inside a pocket is the main goal of this thesis. For that, some topics have to be further explored. We do this in the next chapter.F

3

State-of-the-art

In the state of the art, we discuss the most related topics to this thesis. These topics are VLC with real-time processing, overcoming NLOS, Wearable VLC, and the combination of VLC and NFC.

3.1. Real-time processing

Works that have built prototypes and real-time processing are relevant to this thesis because of its goal to find a practical solution to a problem.

Videv et al. published a paper that dealt with the real-time processing part of VLC, they demonstrated a real-time processing proof of concept using Spatial Shift Keying (SSK) [33]. The authors used 4 of the 24 LEDs to transmit the data, and 4 photodiodes to receive the data. The reason that the authors did not include all LEDs is because of the principle feasibility of SSK. A combination of BeagleBone and an FPGA was used at the transmitter and receiver's side. This made the setup quite expensive (100eu+), including the photodiodes. The authors achieved a data rate of 0.93 Mbps with a BER of 2x10-3.

Li et al. developed a high-speed system with low complexity. The authors reached a data rate of 550 Mbit/s at a distance of 60cm with a BER of 2.6 x 10-9 by tweaking the resistors and capacitors in their VLC pre-emphasis and post-equalization circuits. However, similar to Videv et al. [33] the authors used expensive components to achieve this. Also, the authors relied on a BER tester to get the experimental results, which is not a practical application device.

Other VLC solutions have focused on mobile phones as receivers [41, 7, 40]. Yang et al. [41] implemented the ReflexCode system by combining traditional amplitude demodulation with slope detection to decode the greyscale modulated signal. By also dynamically changing the threshold depending on the symbol distribution, they demonstrated that it can reach 3.2kb/s at a distance of 3m. In this thesis, we get some inspiration for their experimental setup.

More recent papers like Hemetkhan et al. investigated the performance of polar, turbo and low-density parity-check codes (LDPC) on a real-time processed VLC link [19]. The paper demonstrates this by transmitting over an additive white Gaussian noise channel in a simulation. Although this is still a simulation, the authors had practical scenarios in mind. These scenarios are the list size for the polar codes and the number of iterations for Turbo and LDPC.

Yang et al. implemented a VLC receiver placed into the audio jack of a mobile phone [42]. Because of the audio jack sampling rate, they only reached a sampling rate of 44.1 kHz. Still, the authors achieved a data rate of 80 kbps because of 8-PAM modulation. To not only limit themselves to getting results using the phone, a microcontroller which can reach a sampling rate of 200khz is also employed. Because of the 8-PAM modulation, a complex transmitter was needed, a PCB with 255 LED chips divided into 8 groups. Multiple experiments have been done, including different frequencies, distances, angles, differences between 4-PAM and 8-PAM, and user mobility.

There are also commercial products for VLC. These include PureLifi, Signify, and Oled- comm [32]. These products can reach 100 Mb/s in a practical environment. However, these are not open source, so details about their implementation cannot be explored.

From the reviewed papers, we found out how they deal with practical environments. This will be taken into account for our implementation. Also, some ideas can be taken to decide the types of experiments needed to evaluate the system. Those two points, however, are not the main topic of this thesis. The novelty of our work is overcoming the limitations of a new type of scenario, as explained next.

3.2. Overcoming NLOS

Overcoming NLOS is a significant challenge for VLC, as data communication is disrupted when the LOS is obstructed. It is also an important aspect of this thesis, so the State of the art of this specific topic should be researched. Scenarios of NLOS situations are illustrated in figure 3.1.

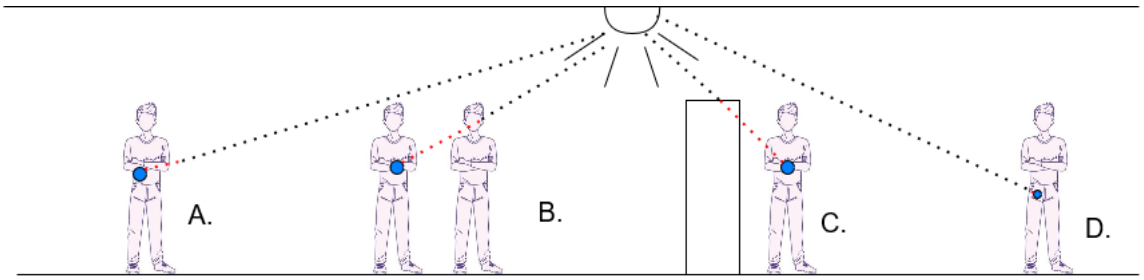

Figure 3.1: Obstruction of VLC: A: the body of the person blocks the LOS, B: Another person blocks the LOS, C: A structure blocks the LOS, D: NLOS because the receiver is inside the pocket

Rodoplu et al. developed a mathematical framework for VLC link availability and a probabilistic model of the VLC network concerning human behaviour in indoor environments [28]. A VLC system simulation was designed to track both static and mobile VLC devices in smart home environments. This paper is one of the first to consider human behaviour in indoor environments.

Dixit et al. also used a simulation to analyse NLOS environments. The authors evaluate the performance of a VLC system by receiving the reflections of a non-LOS VLC channel. The transmitter was static, and three receivers were placed at different locations. By changing the number of reflections and having three different receiver locations, they calculated the BER of the receivers in different environments.

A similar paper is completed by Singh et al. The authors analysed the performance of a VLC system by using a geometry model-based approach to analyse the performance of an indoor VLC link that included human blockages [29]. They compared the system with two alternatives, 4 or 8 transmitter LEDs, both with the same total power constraint. It was discovered that the 4-LED configuration performed better than the 8-LED configuration when there was a lower density of human blockages in the room. However, when a higher density was presented, the 8-led configuration performed better.

The above papers obtained their results with simulations but not with experiments. Cui et al. received the VLC data with the side RF channel created by the VLC [11]. An RF side channel is created because of the switching MOSFET's in the transmitter. They can receive these signals with specialized coils and decode the VLC data. They evaluated their system by experimenting with different scenarios and could communicate in a MIMO scenario.

The most related paper to this thesis is done by Beyens et al. [4]. The authors address the issue of having human bodies blocking the VLC link. In this paper, The user was guided by the system to rotate themselves in the right direction to get a working VLC link. By having 9 transmitters and 4 receivers, the authors evaluated their implementation with experiments. There are still some limitations, including the willingness of users and visual feedback on the required rotation needed to get the optimal orientation.

Almost none of these papers have considered the extreme NLOS situation of having the receiver put in a pocket. Only the solution of Cui et al. will work in this NLOS situation because it does not need the LOS. However, their solution will not fit in an small space like a pocket.

3.3. Wearable VLC

Since a wearable solution is to be designed, we research the state of the art of wearable VLC. Understanding existing techniques could help identify potential challenges and innovative practices that could be applied to this thesis. Wearable VLC is a topic that has received limited interest and is a reason why this topic was chosen for this thesis.

The first paper that deals with wearable VLC is done by Adiono et al. [1]. They designed a wearable patient monitoring device. This device helps the doctor by providing the patient's conditions in a real-time manner. It consists of 2 VLC parts, a patient and a coordinator device. The patient device is the VLC system worn by the patient and equipped with IR (infrared) for the uplink. The Coordinator device has an LED driver and an IR receiver. It can communicate with the patient's device via a VLC link, and the patient's device can respond with IR. The use of VLC in this medical context is beneficial because it does not cause any electromagnetic interference, which is a critical consideration in sensitive environments such as this. OOK modulation was chosen because a high data rate was not needed. To communicate correctly between devices, A MAC layer is added to ensure reliable communication. However, the system's performance is optimal only within a range of 110 cm between the LED and photodiode, and the study lacks crucial experiments related to mobility.

Cui et al. did not utilize VLC to communicate data, instead, they harvested the RF energy sent via a VLC transmitter[10]. The authors used the techniques presented in [11] by taking advantage of the RF side channel that the switching MOSFETs of the VLC transmitter produce. With this wearable device, they harvest energy which could for example be used to read out sensors. This approach highlights the potential of wearable VLC technology beyond just data communication.

Another notable contribution to wearable VLC is the study by [6], which focuses on a wearable backpack designed to assist blind, or visually impaired individuals manoeuvre through a hall. This system uses VLC to transmit positioning information, achieving a data rate of up to 100 kbps with VPPM and a Field of View of 53 degrees. The VLC system is used to send information about the position of the backpack. The authors claim that they have a working VLC link, the paper, however, lacks any experimental results about the VLC component itself. The experiments focus solely on different users navigating the hallway by evaluating if the correct path is taken. The backpack system is limited to only navigation assistance and does not integrate with a smartphone, which this thesis will focus on.

While wearable VLC is still in its early stages, existing studies demonstrate the potential for diverse applications, from healthcare to navigation and energy harvesting. However, none of these papers have included a combination with another technology to send the VLC data obtained to a mobile phone in a pocket.

3.4. Combination of VLC and NFC

In this last section, we research the state of the art for combining VLC and NFC. Similar to wearable VLC, this topic has rarely been explored. Given that this thesis implements a combination of VLC and NFC, reviewing the relevant papers might provide valuable insights.

Liu et al. wrote one of the first papers that researched a combination of RFID, fluorescent light communication (FLC) and Bluetooth [24]. They propose a self-positioning method by combining the three communication modes to obtain enough information to position the user accurately. With position detection software, the authors computed the distance from the FLC receiver to each receptive fluorescent light with the FLC link with a communication speed of 9600 bps. The RFID is used to complete the local position by putting RFID tags in each Fluorescent light. If the user is close enough, it will detect the RFID tag and know which location the user is in. However, the authors do not use the RFID or the FLC to be able to transmit data and the system does not connect to a mobile phone.

A combination of VLC and NFC is achieved by Wang et al. [34]. In their work, they enable passive RFID tags to receive VLC messages. An augmented battery-free RFID tag with an added photodiode is designed to detect light switching. The RFID scanner and the VLC transmit simultaneously, the VLC then adds contents to the RFID response to make the return message unique. Its VLC system can decode messages up to 100 bits. Despite its innovative approach, this system is focused primarily on object localization and verification of identity rather than high-speed data transfer. It also does not

interface with mobile devices.

In conclusion, the combination of VLC and NFC remains underexplored. The existing research primarily focuses on specialized applications such as positioning and localization. However, none of the papers have tried to combine their implementation with a high-speed VLC system that can connect to a mobile phone. This thesis aims to bridge this gap by developing a system that not only combines VLC and NFC but also uses it to enable fast VLC data to be reached by an enclosed receiver.

3.5. State-of-the-art conclusion

In this chapter, we have explored the state of the art in related topics, including real-time capabilities, Losing Line-of-Sight, Wearable VLC, and the combination of VLC and NFC.

We find out how to deal with a real-time VLC system, and we borrow some ideas and metrics to determine how to evaluate our solution. As for the NLOS, some interesting papers have tackled this problem. However, almost none have considered the case of having the receiver in an enclosed space. The one that could but had not been considered would have failed to design a compact solution suitable that works in an enclosed space.

Wearable VLC is still in its early stages, existing papers explore the use of wearable VLC, but this is mostly done in medical environments. None of them have included a combination of other technologies.

The combination of VLC and NFC has been researched in the context of object localization and identity verification. None of the existing studies have yet realized a high-speed VLC that can stream its data to an enclosed receiver via NFC.

This thesis aims to address these gaps by developing a wearable VLC system that combines VLC and NFC to enable reliable communication even when the receiver is in an enclosed space like a pocket. Mobile phones spend most of their lives in pockets, so this line of research must be explored.

4

System overview

In this chapter, we describe LightVest's system overview. First, the problem statement is recapped, and the system requirements are set. Then, the thesis system is given an overview of all its important components. In the next chapters, these components are explained in more detail.

4.1. Problem statement

The primary challenge we address in this thesis is a system implementation that enables the reception of VLC data even when the receiver is located in a pocket. Typically, VLC systems require a direct line of sight (LOS) between the transmitter and receiver to function effectively. However, in some scenarios, the receiver may be obstructed or placed in an enclosed environment, such as inside a pocket or a bag, which disrupts the direct optical path and prevents efficient data transmission.

This means that a system needs to be implemented in which the VLC data can still be received even though the original receiver is in a pocket.

4.2. Requirements

This implementation would need some requirements to consider this system successful.

- **Range of 1.5 meters:** The LightVest will be used in indoor environments such as offices or warehouses, as explained in the introduction. In those places, the lightning infrastructure already exists, and these lights can be used to transmit data through VLC. We assume that the lights are placed evenly and that the distance between the receiver and transmitter is always under 1.5 meters. It could still be possible to receive from greater distances, but the efficiency may be lower.
- **Flickering not visible** The light of the VLC transmitter should not cause any flicker. This means that the frequency of the VLC transmitter should be at least 500 Hz [12].
- **Security of VLC still in mind:** Because the received data needs to be sent to the enclosed receiver wirelessly, a problem could arise that the system is not as secure as VLC natively is. So this is something to be considered when searching for wireless communications to stream to the enclosed receiver.

4.3. The LightVest System

The system that has been designed is **LightVest**. In this system, the receiver in the pocket will not receive the VLC data directly. The light of the VLC is picked up by additional photodiodes that are placed on a vest, these will be in the LOS of the transmitter. The values of the photodiodes are processed and then streamlined to the receiver in the pocket via an NFC connection. This system has four key components: the VLC Link, an MCU, the NFC Link, and an Android system. The overview is visualized in figure 4.1a, and in figure 4.1b, the fully developed system can be seen.

The functionality of each component is detailed below:

VLC Link: The VLC link consists of a transmitter and the receivers on the vest. On the transmitter side, an LED is modulated to transmit VLC data to the receivers, which are photodiodes. The photodiodes receive the data and send it to the microcontroller to further process it.

MCU: The microprocessor unit demodulates the signals from the photodiodes. Then, the demodulated data is further processed and sent to the Android system via the NFC link.

NFC Link: The NFC link is responsible for streaming the VLC data. It consists of a writable tag and can be written and read by the MCU and the phone.

Android system: The Android system consists of a phone and an application. The application is implemented to enable the phone to receive the data from the NFC link. Also, multiple different modes on the MCU could be launched from the application.

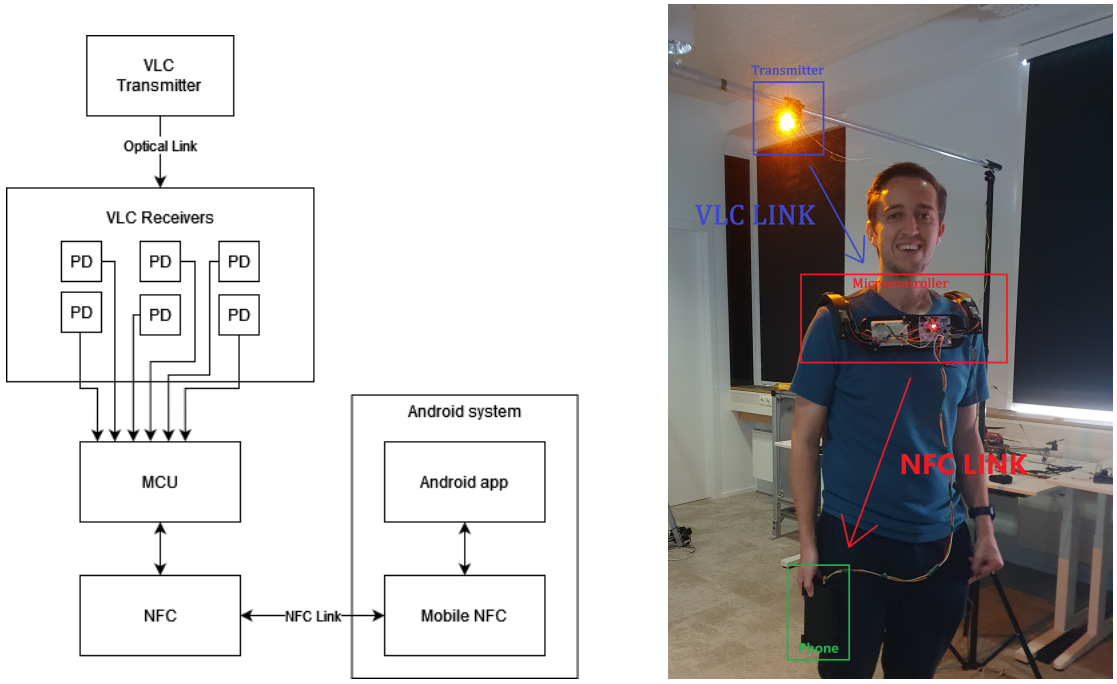

(a) System Overview

(b) System in picture

Figure 4.1: LightVest system overview: On the left, the system. On the right, the fully implemented system

4.4. Process

In this section, We explain the typical process of how the LightVest system operates. It is described below and visualized through flowcharts in figure 4.2.

1. First, the VLC transmitter modulates and sends a package of 1 to 255 bytes. This package includes preamble, length, message and CRC.
2. The processing unit receives the signals of the photodiodes with the use of ADC's. The data is demodulated and decoded in real-time.
3. When a full package is received, the CRC is checked to see if the package is delivered correctly and the data is sent to the NFC tag through I2C.
4. At the same time, the NFC reader on the Android system's side constantly checks if a message has been put into the NFC tag. When it detects that the tag has been updated, the system will read the data out of the NFC tag.
5. The data is processed in the Android app, this can be done in various forms depending on what kind of mode is requested.
6. When the NFC tag is read, a GPIO pin is triggered at the processor unit. This is useful because the processor unit knows when a new message can be put into the NFC tag.

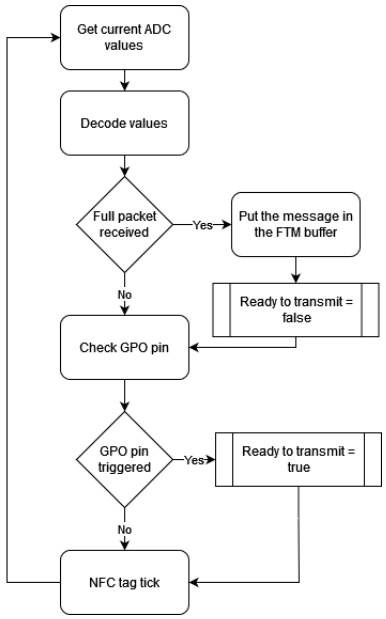

(a) Flowchart of the code running on the microcontroller

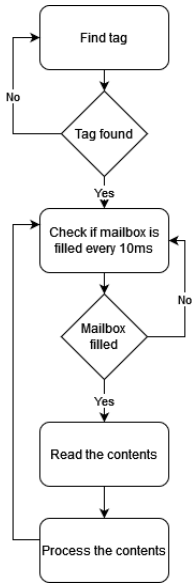

(b) Flowchart of the code running on the android phone

Figure 4.2: Flowcharts of the LightVest system

In almost all the steps, we faced some challenges that had to be tackled and dealt with. For example, the method by which we demodulated the received signal or how we improved the current performance of the NFC link. We will discuss these in more detail in the next two chapters: the VLC link and the NFC link.

5

VLC link

In this chapter, we cover all the aspects of the VLC link. This includes the transmitter, the receiver, the (de)modulation, the packet description, a study to find the best PD angles, optimization of the VLC link, and the evaluation of the VLC link.

5.1. Transmitter

5.1.1. Light source

As we have explained in the background chapter, an LED is used as the light source for the transmitter. The LED has the following specifications, which can be seen in table 5.1.

DC forward current	350 mA
Typical flux	50 lm
Forward voltage	2.2V
Viewing Angle degree	135

Table 5.1: LED specifications

In further research, a brighter LED could be used to match an office setting. This LED's power is significantly lower than the lights found in normal office environments.

5.1.2. Transmitter hardware

To transmit data, the light needs to be modulated. The modulation technique is explained later, but the important requirement is that the LED is switched on and off at a very high speed. The high data rate is not the scope of this paper, but we do want to try a data rate of at least 10 kbps. To achieve this, a switching frequency of 20 kHz is needed.

Our transmitter hardware consists of a microcontroller, a MOSFET driver, a MOSFET, and a current limiter.

The microcontroller is responsible for modulating the signal by driving a GPIO pin to turn a MOSFET on and off. The MOSFET driver is required to switch the MOSFET more efficiently, as a GPIO pin alone lacks sufficient current and suffers from slow rise and fall times. The MOSFET can deal with the power differences caused by the switching of the LED. A current limiter controls the current flowing through the LED, as the brightness of the LED is related to the current.

We use Arduino DUE for the microcontroller. This microcontroller is utilized to get the first prototype working, and it is deemed fast enough for the total of the thesis. It has a maximum clock speed of 84 MHz. Using a timer of 1 MHz, we were able to switch at a maximum speed of 500 kHz, which was fast enough for the current scope of our thesis.

For the MOSFET driver, we selected the EL7104CNZ. This has a rise and fall time of 20ns (50 MHz),

ensuring it can handle high-frequency switching. The same can be said about the MOSFET, which is the IRLB4132PBF. Here, the rise and fall times are 92ns (10.8 MHz) and 36ns (27.8 MHz), respectively. This meant that we were able to switch with a maximum speed of 10.8 MHz, which is more than enough for our thesis.

The LED is powered by a 15V 1.6A power adapter. To limit the current, a high-wattage resistor of 19,5 Ohm is added. This way, the LED was driven by a current of 615.3 mA.

The hardware schematics can be seen in figure 5.1a, and a picture of the hardware is seen in figure 5.1b.

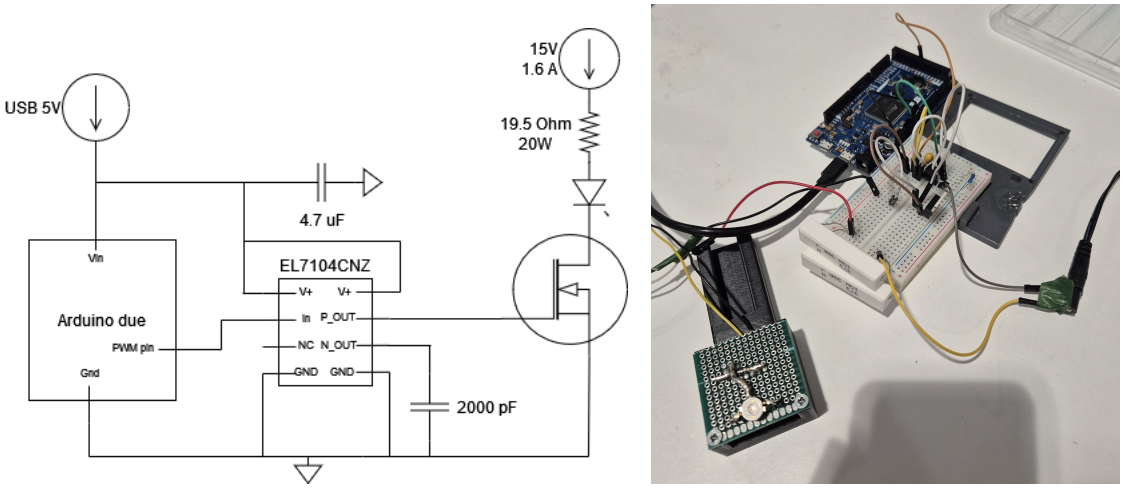

(a) Schematics of the transmitter hardware

(b) Hardware of the transmitter

Figure 5.1: Angle experiment

5.2. Receiver

In this section, we explain the details of our receiver. This receiver consists of the photodiodes, the microcontroller and a 3D model.

5.2.1. Photodiodes

As explained in the background section 2.2.1, photodiodes are commonly utilized because of their high bandwidth and simplicity. To not spend much time researching for photodiodes to get a first prototype working, the OPT101 is selected, as it is a useful module with a photodiode and an amplifier in one chip.

The specifications of the OPT101 can be found in table 5.2.

Photodiode area	5.2 mm2
Bandwidth	23 kHz (At 10 Vpp)
Current responsivity	0.45 A/W

Table 5.2: OPT101 specifications [21]

The photodiodes are connected to the analogue input from the microcontroller, which processes and demodulates the receiving Link.

5.2.2. Microcontroller

The microcontroller is responsible for receiving the values from the photodiodes, processing the signals by demodulation and decoding, and then transferring the data to the NFC tag.

Requirements are established before choosing a microcontroller. These include:

- **A minimum of 6 ADC inputs:** Since there are six or more photodiodes, the microcontroller must support at least six ADC inputs.

- **High performance:** Due to the constant need for signal demodulation, which is computationally intensive, a high-performance microcontroller is essential for achieving a high data rate.
- **Power consumption:** In this thesis, we propose a wearable solution, so the power consumption cannot be too high.

The STM32F446RET is selected as the microcontroller. This is a cost-effective and easy-to-use microcontroller. Given the focus of this thesis on rapidly developing a functional VLC system, this microcontroller met all the necessary specifications, so other alternatives were not considered. The specifications of the STM32F446RET are listed in table 5.3.

Clock speed	160 MHz
ADC's	16 ADC channels
Maximum ADC clock speed	40 MHz
Maximum I2C clock speed	400 kHz

Table 5.3: STM32F446RET specifications [30]

The software development for this microcontroller is programmed with Rust.

5.2.3. 3D model

A 3D model is designed and realized to showcase and test the system. This was our first experience with 3D modelling, and it was done using Autodesk Fusion. The 3D-printed model is wearable and includes six locations for the photodiodes. It also has mounts for securely attaching the microcontroller and breadboard with screws. The final 3d Model design and realization can be seen in figure 5.2.

(a) 3D LightVest design

(b) 3D Printed LightVest design

Figure 5.2: 3D design and the printed 3D model of the Vest

5.3. (De)Modulation

5.3.1. Modulation

The signal modulation is performed using an Arduino Due. As stated in the background 2.3, maximizing the data rate is not the goal of this thesis, so OOK modulation with Manchester encoding is chosen because of its ease of use. Bits are represented by transitions: a transition from high to low represents a '0', and a transition from low to high represents a '1'. This is a useful modulation because it does not cause flickering and does not require synchronization. In figure 5.3, it illustrates how Manchester encoding works.

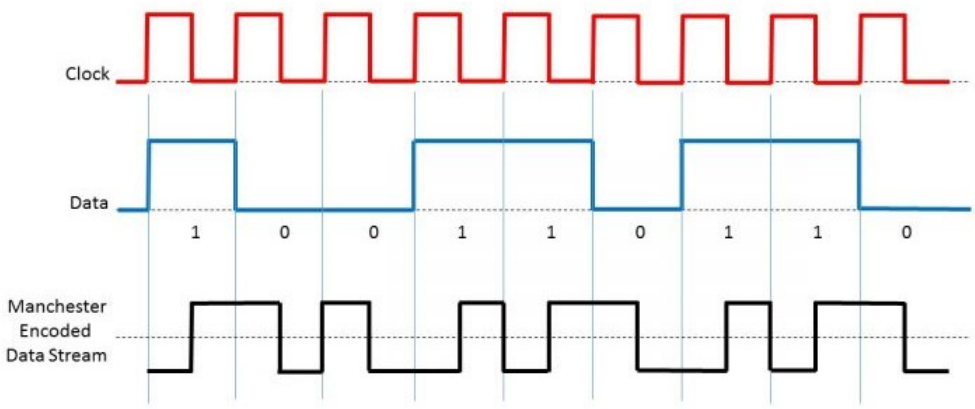

Figure 5.3: Workings of Manchester encoding

5.3.2. Demodulation

The demodulation process is performed in real time and consists of multiple stages. At each sample, the software checks whether a transition from high to low or the other way around has taken place. This is checked using a threshold value, the way we update this value is explained later in section 5.6.2. When the signal crosses this threshold, it means that a transition has taken place, and the demodulation can get started. We use two key values during demodulation:

- **Level array:** An array of two values that keep track of the signal levels, used to determine a bit.
- **Half symbol counter:** Keeps track of the amount of half symbols, used to know when a bit can be determined.

The demodulation stages are as follows:

1. **Threshold crossing:** Checks if the signal has crossed the threshold, if it did, the process proceeds to the next stage.
2. **Symbol checking:** The number of samples between threshold crossings is evaluated. If it exceeds 3/4 of a symbol, it indicates that a symbol has passed. The current signal levels are stored in the level array, and the half-symbol counter is increased by two. If the symbol counter is between 1/4 and 3/4 of a symbol, it indicates that only a half symbol has passed, so the half symbol counter is incremented by one and the current signal level is stored in the In both cases, the amount of samples has been reset to zero, and the current signal level is stored in the level array, using the half symbol counter as an index. The process continues to the next stage.
3. **Bit determination:** The bit determination is done by checking the half symbol counter. If the counter is bigger or equal than 2, a full symbol has passed. The half symbol counter is reset to zero, and a bit can be determined. A [0, 1] in the signal state array indicates a bit value of 1 (low to high transition), while [1, 0] indicates a bit value of 0 (high to low transition). If the value state counter is 3, the half symbol counter is reset to one because a new symbol has already started. After this, the process returns to the first stage.

If the number of samples has exceeded 1.5 symbols and no threshold crossing has occurred, we initiate an idle time, resetting the demodulation process.

5.4. Packet

The packet consists of multiple fields: preamble, length, message, and CRC. The structure of the packet is illustrated in figure 5.4, and an example with actual values from the photodiodes is shown in figure 5.5.

Preamble (2B)	Length (1B)	Message (0..255B)	CRC (1B)

Figure 5.4: Packet

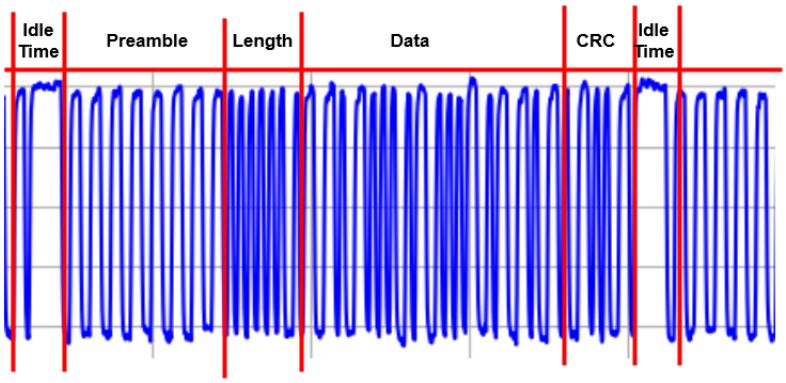

Figure 5.5: Packet that has been received

The **preamble** is a crucial sequence used to detect the start of a data transmission. Two bytes with a value of 0xAA are chosen because this gives a sequence of full periods in Manchester decoding, minimizing the noise at the start of a packet.
Length indicates the size of the message. Since it's only one byte, the message has a maximum length of 255 bytes.
The **message** field contains the data to be transmitted. It can have a maximum length of 255 bytes, as specified by the length field.
The **CRC** field will check if any error occurred during the transferring of data. By calculating its value using the bytes that have been received and comparing it to the received CRC byte, it can determine if the package has been sent correctly.

The software processes the packet using a state machine. When something goes wrong during a packet, the state will be reset to the Preamble state. The Preamble should be found again after an idle time and the packet can be processed. The message is further processed when a packet is fully received and the CRC is correct. Eventually, it is sent to the mobile phone through the NFC link. This process will be explained in the next chapter.

5.5. Determining best positions and angles

Light propagates in a Lambertian pattern, which means that the angle and orientation of the transmitter and receiver influence the total received power. To find the best-performing angle of our photodiodes, we have two tasks. First, we explain the Lambertian propagation model, which is then used to calculate the best-performing position and angle with a simulator and an experiment.

5.5.1. Lambertian propagation model

Lambertian propagation is a mathematical model that describes the propagation of light [22]. With this model, the received power at a photodiode can be calculated with the following formula:

$$\text{Received power: } P_r = P_t \cdot H(0) \cdot G_r(\alpha) + N \tag{5.1}$$

In this formula, P_t is the transmitter power, N is the added Noise, $G_r(\alpha)$ is the filter gain of the PD, and $H(0)$ is the channel DC gain. All these values are constants based on the angle between the receiver and the transmitter, except for the channel DC gain, this is not a constant. The channel DC gain can be calculated using the formula:

$$\text{Channel DC gain: } H(0) = A_{rx} \cdot \frac{m+1}{2\pi \cdot d^2} \cdot cos(\alpha)^m \cdot cos(\phi) \tag{5.2}$$

$$\text{Lambertian order: } m = \frac{-ln(2)}{ln(cos(\phi_{1/2}))} \tag{5.3}$$

In this formula, A_{rx} is the Photodiode sensing area, d is the distance between the transmitter and the receiver, α is the angle of the photodiode compared to the transmitter, and ϕ is the angle of the transmitter compared to the photodiode. At last, m is the Lambertian order, which depicts the angle at which the transmitter can light up ($\phi_{1/2}$). In figure 5.6 the angle denotations are shown to make it more readable.

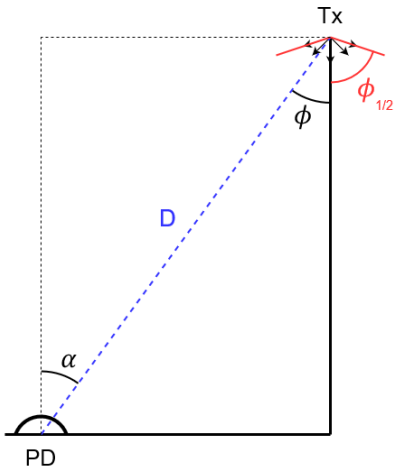

Figure 5.6: Lambertian model

5.5.2. Simulation

The 2D simulation is created in Python to calculate the optimal angle to place the photodiodes, using the former formulas. The transmitter is placed at a static place, at coordinates [0,1]. The receiver is equipped with 3 photodiodes, one in the middle with an angle of 90 degrees and two on the left and right that mirror each other, of which the angle is adjustable from 0 to 90 degrees. The receiver follows a path that runs from x=-5 to x=5, with steps of 0.1, all at a height of y=0. At each step, the received power is calculated for every photodiode. It is also important that the blockage of the vest itself is taken into

account, so it is decided that when the angle reaches more than -50 and 50 degrees, the received power is set to 0.

An example of the received power over a path can be when the adjustable photodiodes are 60 degrees and are visualized in figure 5.7. In this figure, one can see that the photodiodes that are placed on the sides perform better the further away they are from the transmitter.

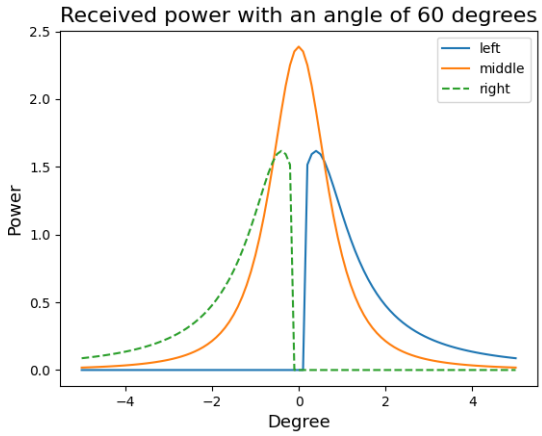

Figure 5.7: Path result when the angle of the photodiodes are 60 and -60 degrees.

The received power over a path can be calculated when the photodiodes on the side have a certain angle. We can now determine the best angle for the photodiodes by computing the total envelope power of each angle over a certain path. For that, we create a new simulation with a Python script that calculates the envelope power of each angle over the same path that is used in figure 5.7.

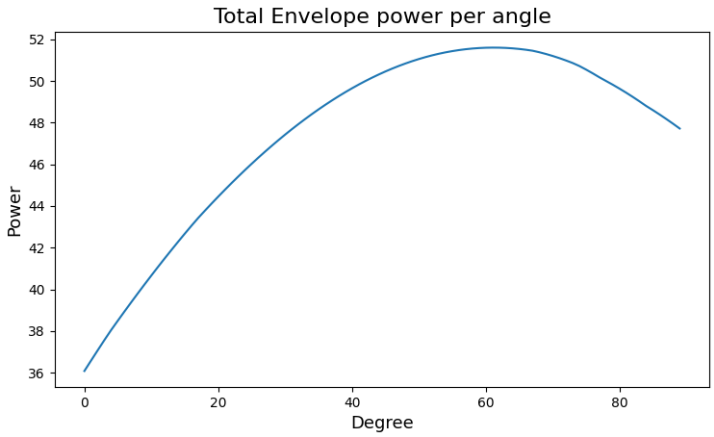

Figure 5.8: Results of the total envelope power per angle degree

The results, which can be seen in figure 5.8, clearly show that a greater angle of the receiver results in a higher envelope power until it reaches about 60 degrees. After that, the envelope power decreases. This happens because the angle gets closer to 90 degrees, and the advantages of having other photodiodes in different angles decrease the total amount of envelope power. With these results, we show that theoretically an angle of **60 degrees** is the best-performing angle.

5.5.3. Angle experiment

From the simulations, an angle of 60 degrees was theoretically the best-performing angle. We wanted to experiment with this in a practical environment. The first step was to design and create a simple 3D model where the photodiodes could be placed at a certain angle. The angles that were chosen are 10, 30, and 60 degrees.

To test this, we designed a 3D model that can hold 7 photodiodes. Three photodiodes are placed tilted on the left, three on the right and one is placed flat on the top. A picture of the 3d design is visible in figure 5.9a.

(a) 3D model used for the angle experiment

(b) Visualization of the angle experiment setup

Figure 5.9: 3D Model and setup for the angle experiment

In this experiment, we almost have the same setup as the simulation. The transmitter is put at a height of 1 meter and the receiver (Being the 3D model) is placed on a path from 1.6m to -1.6m. A visualization of the experiment can be seen in figure 5.9b. We begin placing the receiver on the left, and in steps, we move it 5 cm to the right. In each step, the BER is calculated for every photodiode. The BER is calculated with packets of 22 bytes and a speed of 5kbps within a timeframe of 10 seconds.

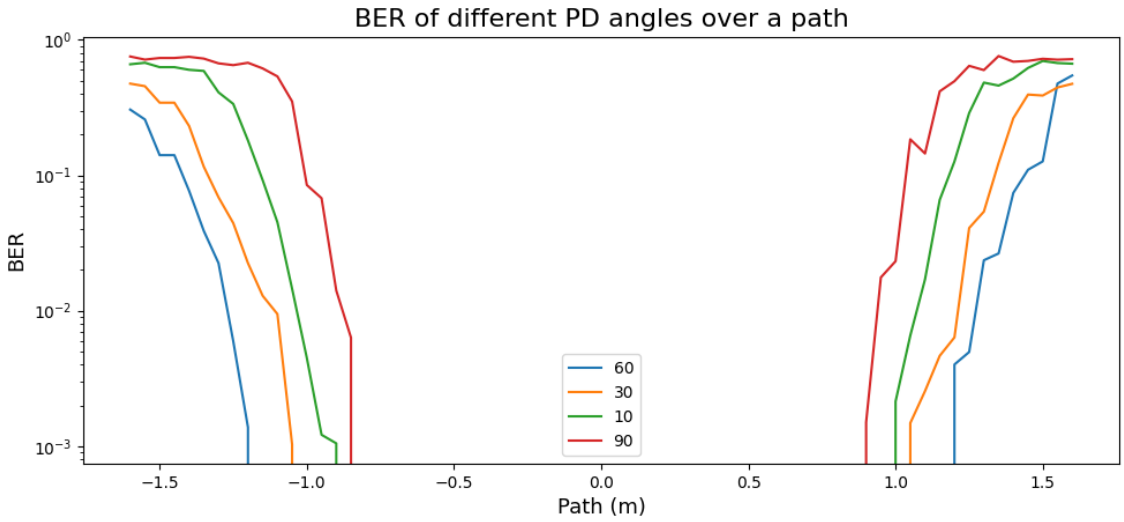

Figure 5.10: Results of the Angle experiment, with degrees of 10, 30, 60, and the photodiode in the middle which is on a 90-degree angle

The results of the experiment are shown in figure 5.10. It shows that an angle of 60 degrees is the best-performing angle. On both sides, it had a BER of 0 at a distance of 1.15 m, while the angle of 30 degrees had a BER of 1.2×10^{-2}. As expected, the angle of 30 degrees was second best, with a BER of 0 at a distance of 1.05 on both sides. The 90-degree photodiode performed the worst, by already breaking down at a distance of 85cm.

After performing a simulation and an experiment to find the best-performing angle, we can determine that an angle of **60 degrees** must be placed on the LightVest to achieve the best performance.

5.6. Improving link performance

Since LightVest is a wearable solution, high mobility is to be expected. With high mobility, a significant variance is introduced. This needs to be taken into account when implementing the demodulation. Multiple measures have been implemented to enhance the VLC link's reliability and data transmission quality to ensure robust demodulation and high performance.

5.6.1. Filtering

The first implementation we use to improve the link performance involves adding a filter. A filter is crucial for reducing noise. The filter that is applied follows the following formula:

$$y[n] = \alpha \times x[n] - (1 - \alpha) \times [n - 1] \tag{5.4}$$

In this equation, α is an important variable because it determines the strength of the filter. To identify the best performing α value of an experiment is done, which can be seen in Appendix A. In this experiment, the transmitter was placed facing downwards at a height of 110 cm. The receiver was placed on the ground, at distances of 25, 50 and 75 cm. The best-performing combination of parameters was determined by increasing the α value from 10 to 60 with steps of 5 and the adaptive threshold value β, explained in the next section, from 0.005 to 0.1 with steps of 0.005.

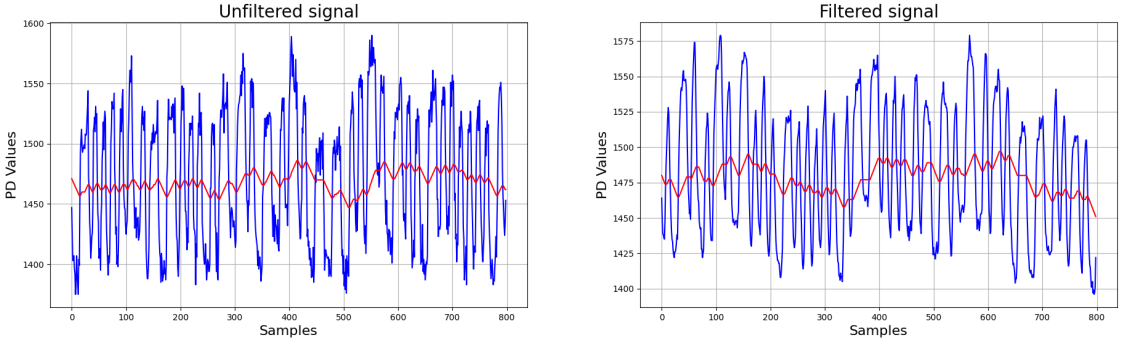

(a) Visualization of a unfiltered signal

(b) Visualization of a filtered signal

Figure 5.11: The image on the left displays a signal without any applied filter, while the image on the right showcases the signal with a filter applied.

We can clearly see the difference between an unfiltered and a filtered signal in figures 5.11a and 5.11b. In the unfiltered signal, errors are more likely to happen because our demodulation process takes place when the threshold (red line) crosses the signal. We can see in figure 5.11a that it sometimes crosses the signal, at times when it is not supposed to. This can result in packets that demodulate at the wrong times, failing the CRC check.

Other filters

Future work could explore other types of filters, such as Infinite Impulse Response (IIR) or Finite Impulse Response (FIR) filters. These filters may offer an improved VLC link. However, they could also demand more computational resources, potentially slowing down the microcontroller's processing power.

5.6.2. Threshold

We use a threshold to determine if a signal changes from high to low or from low to high. This is an important step when one uses Manchester encoding. This section explains the methodology used to implement and adapt this threshold.

Adaptive threshold

We update the threshold value each time we process a sample. Traditionally, the threshold is determined by calculating the average value during the preamble and then using this value throughout the whole packet. However, this can be very harmful to the VLC link when a movement is involved. For example,

in figure 5.12 the signal significantly changes during a packet. Normally, this packet would have failed, but with the adaptive threshold, it can demodulate it.

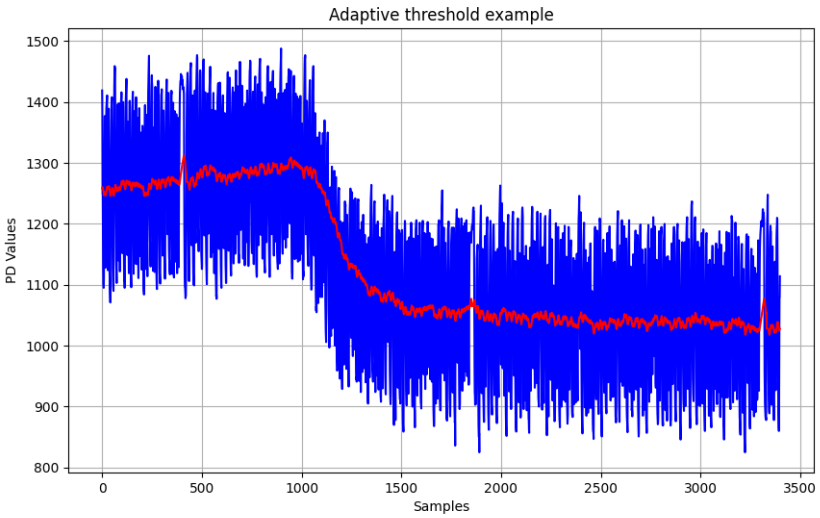

Figure 5.12: Figure showing why adaptive threshold is needed

The adaptive threshold that we implemented is a moving average filter. We calculate this using the following equation:

$$Threshold = (CurrentPDvalue - threshold) \times \beta + threshold \tag{5.5}$$

To determine the value for β we carry out an experiment which is explained in section 5.6.1. Here, the most optimal combination of filter and adaptive threshold value is determined. It can be found in Appendix A.

Resetting threshold

After a packet is completed, an idle time occurs in which the received signal remains high. In this period, the adaptive threshold tends to increase during this idle time to the point that it reaches the signal before a new packet is started. This scenario can hinder the detection of the initial incoming bit, as demonstrated in figure 5.13a.

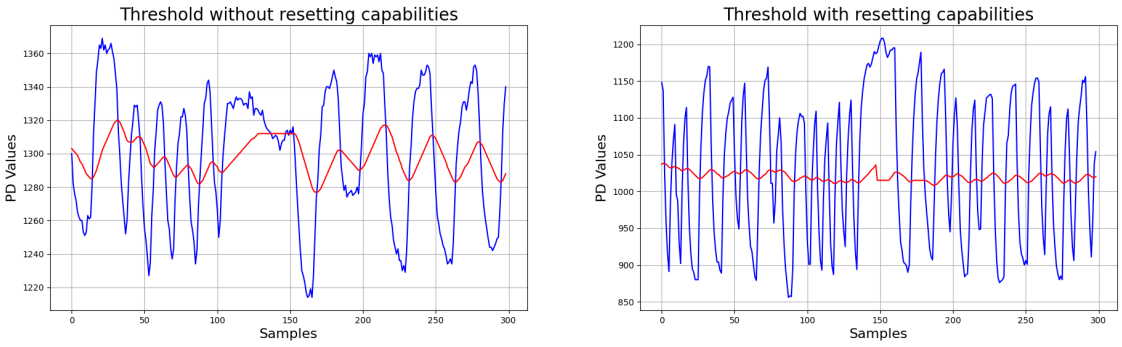

(a) By not resetting, the threshold came into contact with the signal before the idle time was over.

(b) By resetting the threshold, it does not come into contact with the signal

Figure 5.13: The image on the left displays a signal without any resetting threshold techniques, while the image on the right showcases a signal with the resetting threshold technique.

We introduce a solution to this problem by saving the threshold value at every threshold crossing. When idle time is detected, the threshold is reset to the saved threshold value. An example of this happening can be visualized in figure 5.13b. With this solution, we are able to have a higher adaptive threshold and a better link performance.

With the filter and the adaptive and reset strategy for the threshold, the VLC link's performance improves, creating more accurate data reception even in fluctuating signal conditions.

5.6.3. Higher sampling rate

A higher sampling rate may improve the link performance by increasing the signal-to-noise ratio (SNR). We achieve this by benchmarking our software, which allows us to find bottlenecks in the code and try to resolve them.

Decoding a sample

In this benchmark, we focus on the processing time of decoding a sample to identify the most time-consuming functions. A timer of 1 ms is used to measure the timing of specific functions. Because some functions may execute in less than a microsecond, we employ a counter that repeats the function 100 times, averaging the total duration to obtain a more accurate measurement.

Decoding a sample includes several functions. These are explained below.

1. **Filter:** Filters the ADC sample.
2. **Threshold:** Updates the adaptive threshold value.
3. **Manchester:** Decodes the Manchester encoded signal.
4. **Bit calculation:** Determines the bits.
5. **Package state machine:** A state machine function to determine the current status of the packet.

The results of the benchmark are shown in table 5.4.

Function	time (ns)
Filter	68
Threshold	6172
Manchester	148
Bit calculation	340
Package state machine	344
Total	7062

Table 5.4: Processing sample benchmark

From this table, it is clear that the threshold function is the most time-consuming. After analysing this function, we discovered the use of a floating point calculation. It still requires a significant amount of computation time despite the microcontroller having a Floating Point Unit (FPU). After converting the floating point operation to a calculation with signed numbers, we reduced the computation time to 936ns, an improvement of 6.59×.

The total duration for processing one sample is 1.836 μs. This means that in an ideal scenario, a sampling rate of 544.4 kHz is possible when no other tasks are running. However, our scenario is not yet optimal because every time we process a sample it involves polling if a new ADC sample is available. In the next section, we address this aspect.

Direct Memory Access

One issue we encountered is the need for polling functions to check if new ADC values are available. At high sampling rates, this could become a bottleneck. We propose a solution by utilizing the direct memory access (DMA) peripheral of the microcontroller.

With DMA, ADC values can be transferred to memory without CPU intervention, allowing ADC samples to be collected in the background while the CPU processes the samples. We operate it as a circular buffer to make sure we do not process the same data. When half of the buffer is filled, an interrupt triggers, letting the microcontroller know it can process new sample data. Another interrupt triggers when the buffer is full so that the second half of the buffer can be processed.

5.7. VLC link evaluation

Now that the design of the VLC link has been fully explained, we evaluate the VLC link's performance.

5.7.1. Communication speed

In this experiment, we evaluate the data rate and range of the VLC link by calculating the BER value of various data rates and distances. We position The LightVest under the transmitter, and the distance between the LightVest and the transmitter is incrementally increased in steps of 10 cm from 80 to 240 cm, the setup is visualized in figure 5.14.

This experiment uses data rates of 1, 2.5, 5, 10, 15, 20, and 25 kbps. At each step, we calculate the BER in a 10-second timeframe. If the preamble is not detected within 2 seconds, the result for the BER is 1. When a BER value is 0, a value of 0.0001 is displayed.

Our hypothesis is that as the data rate increases, the effective range decreases.

Figure 5.14: Setup picture of the distance vs datarate experiment

The results in figure 5.15 confirm our hypothesis that higher data rates correlate with shorter ranges. At 25 kbps, the data transmission was possible up to 80 cm, but with a high BER of 0.41. At that distance, 20 kbps has a BER of 0.03, and for 15 kbps and below, the BER was 0. the data rate of 15 kbps rate shows a noticeable increase in BER to 3.3×10^{-2} at 120 cm and could not detect the preamble beyond 190 cm. Data rates of 10, 5, and 2.5 kbps maintained a BER of 0 up to distances of 160 cm, 190 cm, and 170 cm, respectively. Despite expectations, 2.5 kbps began encountering errors at 170, potentially due to demodulation issues. At 240 cm, 5 and 2.5 kbps maintained data transmission with BER's of 0.3 and 0.1, respectively.

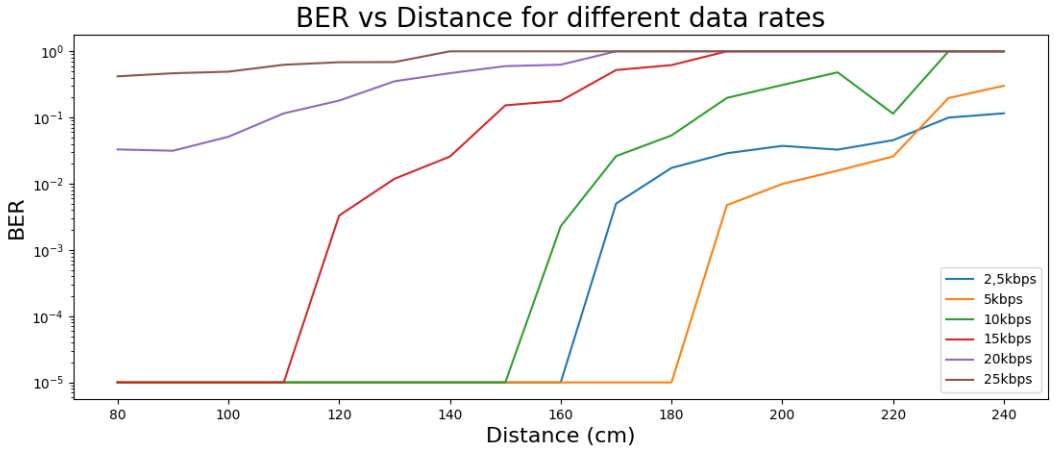

Figure 5.15: Experiment results of the distance vs different data rates.

6

NFC Link

In this chapter, we describe the NFC link to the phone. This is done by looking at the most efficient way to transfer the data. But first, the reason for choosing NFC is described.

6.1. Why NFC

The challenge is to find a solution to the problem of having the receiver inside a pocket. Receiving the VLC data is discussed in Chapter 4, but it is also important to look at which technique is used to transfer the data from the external surface of the vest to the enclosed pocket. Some requirements need to be set to find the right technique, these are:

- **High Data rate:** The communication technique requires a high data rate, preferably one faster than the VLC link data rate (20kbps).
- **Security properties of VLC:** The technique needs to have the security properties of VLC in mind. The VLC data should not be available behind a wall or available to nearby sniffers.
- **Power efficient:** Because this thesis focuses on a wearable device, it is important that the technique is power efficient.

The first thought on how to attack this problem is a USB wire. It has a high data rate and is very power efficient. In truth, it has better security properties than VLC since it does not use wireless communication. However, the solution is not practical. Realistically, it is not useful to ask the user to connect the phone to a USB port inside the pocket. Also, the port would damage quickly due to the frequent connections and disconnections

Considering the above limitation, we determine that a wireless solution is needed. A few options come to mind: Wi-Fi, Bluetooth, and NFC.

Wi-Fi is not an option because of its poor security properties. It is also not power efficient (5-20 Watts) and requires complex hardware. Nevertheless, the range is too big (up to 40 m) and contributes to an already crowded RF.

The same can be said about Bluetooth. The data rate is lower, but its power consumption is also lower than that of Wi-Fi, 1 Watt, and can even be reduced further to 10- 100 mW with Bluetooth Low Energy.

NFC satisfies all the needs. It is very power efficient (under 100 mW), and more importantly, still has the security properties of VLC because its maximum distance is 10 cm. Its data rate is lower, but having a data rate of 424 kbps is enough for the current implementation. Further research is needed to compete with the state-of-the-art data rates. Although NFC performs well in several aspects, its practicality is limited by its operational range of 10 cm. While this short range enhances security, it poses a challenge as the receiver may easily fall out of range. Fortunately, recent research has focussed on integrating NFC antennas in clothing [13, 3, 14, 15, 39]. This demonstrates the feasibility and benefits of our approach. These studies address various aspects, including the design and implementation of NFC antennas in

fabric, ensuring that the technology remains effective while maintaining the comfort and durability of the clothing.

Considering these factors, NFC was chosen to streamline the VLC data transmission to the phone.

6.2. NFC implementation

In this section, we provide a detailed explanation of the NFC implementation, covering both the transmitter and the receiver components.

6.2.1. NFC transmitter

The NFC transmitter required a design that could interface effectively with an MCU while being cost-effective and not overly complex. After we evaluated various options, the solution chosen was the ST25DV64KC, a dynamic RFID/NFC tag from STM. This tag can be written and read to/from by an MCU, is fairly cheap (0.78 euros) and is not complex, requiring only an I2C connection. The chip is also offered as a development board, the X-NUCLEO-NFC07A1 [31]. This board is selected due to its compatibility and ease of integration with the STM32 development board.

The dynamic RFID/NFC tag chip offers 64kB of data in its EEPROM, allowing significant amounts of data to be stored and transferred to a mobile phone. The chip can be controlled with an I2C connection and offers a general-purpose output (GPO) that can be programmed to do various things. However, the chip has a useful feature called the fast transfer mode, illustrated in figure 6.1.

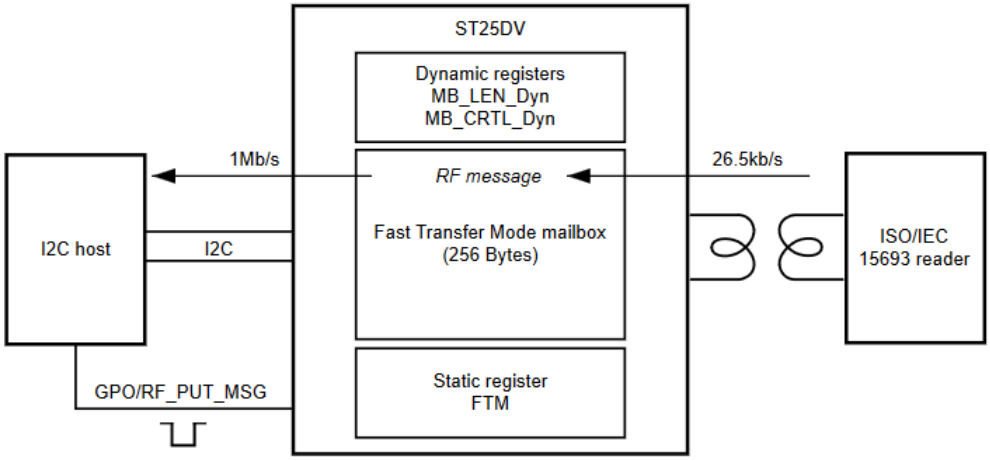

Figure 6.1: Fast transfer mode of the ST25

The FTM enables a theoretical data transfer rate of up to 26 kbps between the MCU and the NFC receiver. In this mode, a buffer of 256 bytes is used to stream the data to the phone. This buffer is called the mailbox, it can be programmed so that the GPO pin notifies the MCU when the mailbox is read by a NFC receiver, allowing the MCU to load new data into the mailbox. It's important to note that the NFC tag cannot notify the phone when data is put into the mailbox. Instead, this must be checked by reading a specific register.

The primary advantage of using FTM is its significantly faster data transfer rate compared to utilizing EEPROM memory. Although the EEPROM has a larger storage capacity, reading 256 bytes takes approximately 320 ms. In contrast, using FTM reduces this time to 81 ms, which represents a 359% increase in data transfer speed.

The software development of the NFC transmitter underwent several stages. At each stage, we made substantial changes to improve the NFC link.

First implementation: sending data via EEPROM
The initial implementation aimed to test the basic functionality of data transfer from the MCU to the NFC tag. The primary focus was to ensure the correct operation of the self-implemented I2C and ST25 drivers. Eventually, we could control the ST25 and store data in its EEPROM. On the Android side, as explained in the next section, we read the data from the EEPROM contents. This marked the initial step in transferring data from the MCU to the phone

Second implementation: Working FTM
The next implementation focused on a functional NFC link between the MCU and the phone with the FTM. Functions were added in the drivers for the I2C and ST25 so that the FTM could be enabled and consequently used.

The FTM implementation worked with the following process. The MCU places the data in the mailbox and waits until the receiver reads it. This process is monitored by polling the GPO pin, which is configured to trigger when the receiver reads the mailbox. When the GPO is triggered, a new message can be put into the mailbox buffer and the process starts over.

However, we found this implementation to be notably slow due to the blocking nature of the I2C operations. Multiple delays were needed to have a successful I2C transmission. This bottleneck meant that ADC samples could not be read during the process. This limitation was fixed in the final implementation.

Final implementation: FTM with non-blocking I2C
In the last implementation, we implemented a non-blocking I2C to fix the problem of delays during an I2C transmission.

This is achieved using a state machine and a non-blocking I2C tick function that progresses through the state machine. The state machine follows the standard I2C transmission protocol with an additional state. The states are visualized in figure 6.2. A buffer that can save up to 10 VLC messages is added so that when I2C fails, the data stream coming from VLC is not disrupted.

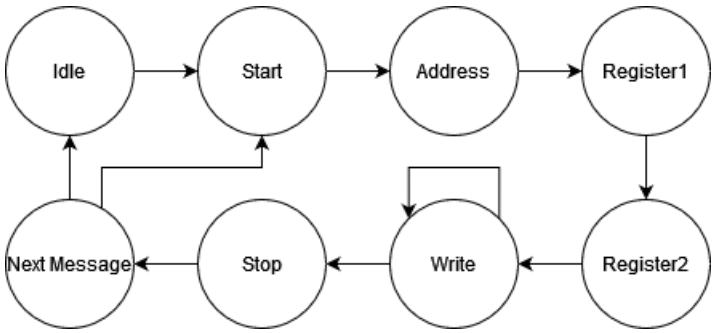

Figure 6.2: I2C states with an extra added state named "Next Message"

The state machine begins in the idle state. When the MCU initiates a data transfer to the mailbox, the state will change to "start", and the protocol follows through the typical I2C states until reaching the "Next Message" state. In that state, it checks if there are any messages in the buffer. If there is a message, the system waits until the mailbox is read, at that point new data is immediately placed into the mailbox.

In each state, it is checked if some I2C error happened during the transmission. For example, a No Acknowledgement (No Ack) scenario can occur if a new I2C transmission starts while the mobile device is still reading the mailbox. When this happens, a No Ack process is started. The I2C transmission is then stopped, and the data is pushed back to the front of the message buffer.

Occasionally, the I2C might become unresponsive without the MCU detecting it. To mitigate this problem, a timeout mechanism is implemented. If the I2C does not respond within a specified period after initiating a transaction, the timeout is triggered, and the I2C is reset to resume normal operation.

Potential best implementation

Even with the non-blocking I2C implementation, the system frequently checks the status of the I2C registers during ADC sampling, which can introduce delays due to branching.

A more efficient approach could involve using an interrupt-based I2C implementation. This method would eliminate the need for continuous checking of the I2C registers. This allows for uninterrupted sample collection and computation for demodulation, thereby improving overall system efficiency.

6.2.2. NFC receiver/Mobile phone

In this thesis, the receiver for the NFC connection is a mobile phone, specifically a Samsung Galaxy S10e. Similar to the NFC transmitter, the receiver implementation went through several stages to reach its final, fully functional form.

Implementation 1: Receiving data from the MCU

The initial implementation aimed to establish a basic connection between the NFC tag and the mobile phone to verify that data could be transferred from the MCU to the phone. To facilitate this, we made use of an application designed by STMicroelectronics, which is available on the Google Play Store[1]. This app enabled us to perform initial tests by reading the contents of the EEPROM from the NFC tag, confirming that the NFC communication setup was working correctly.

Implementation 2: Receiving data through FTM

Following the successful connection and data retrieval from the EEPROM, the next step was to leverage the Fast Transfer Mode (FTM) for more efficient data transfer. For this, an Android application was developed using Android Studio. This application enabled the phone to connect with the NFC tag and periodically poll every 10 ms to check if the mailbox buffer contained new data. When it did, the data was read and the is further processed. In this case, it was displayed on the mobile phone. With this setup, we reached a data rate of up to 21000 kbps.

Implementation 3: Control and Debugging through Application Menus

With a stable connection established, we aimed to utilize the mobile application to control the MCU, thereby speeding up the debugging process for improving the VLC link.

This involved adding menu options that enabled us to test or debug different functionalities, and we could run the experiments more easily. The application interface is visualized in figure 6.3a and includes the following menu options:

- **Try to connect:** In this option, the tag can be connected to the phone by disabling and enabling NFC.
- **Stream VLC:** Contains the functionality from the previous implementation, enabling VLC streaming to the phone, and displaying the received data with text.
- **Graph values:** Visualizes the PD's values and thresholds. By providing a graphical representation of how signals are being received.
- **Get VLC BER:** Retrieves the Bit Error Rate (BER) of the VLC link, using the NFC connection to transfer the results.
- **Vest Experiment:** Tests the LightVest by measuring data and packet success rate over time. The time is determined by clicking a button on the LightVest. This application can be seen in figure 6.3b.
- **NFC Experiment:** Enables only the NFC link by excluding VLC.

[1] https://play.google.com/store/apps/details?id=com.st.st25nfc&hl=nl&pli=1

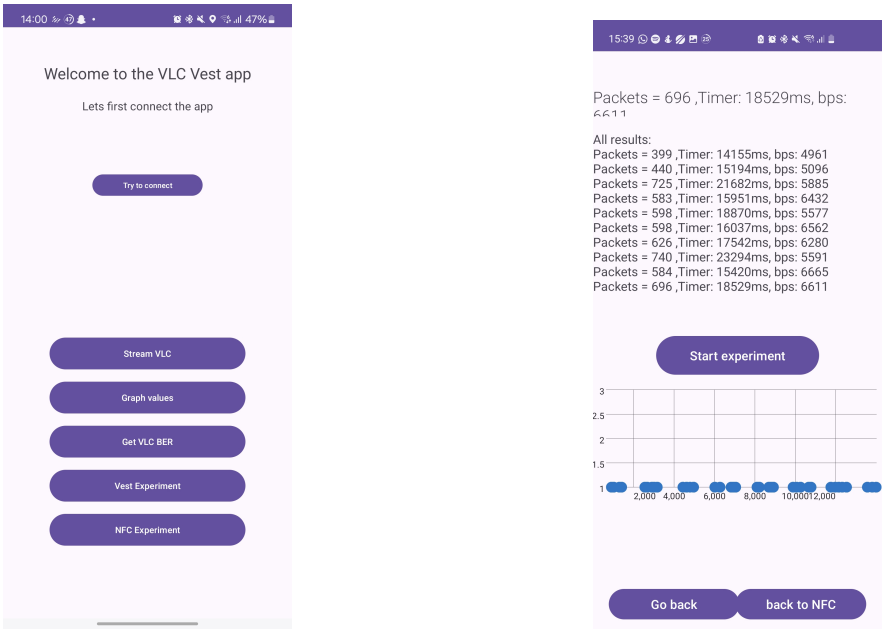

(a) Screenshot of the menu in the application

(b) Screenshot of the Vest Experiment

Figure 6.3: Screenshots of the Android application

6.2.3. Phone holder 3D print

To provide a practical solution for connecting the NFC tag with the Samsung S10e phone, a custom 3D-printed holder was designed. This holder ensures a secure fit for the phone while maintaining reliable NFC connectivity. The 3D model and the final printed holder are shown in figure 6.4.

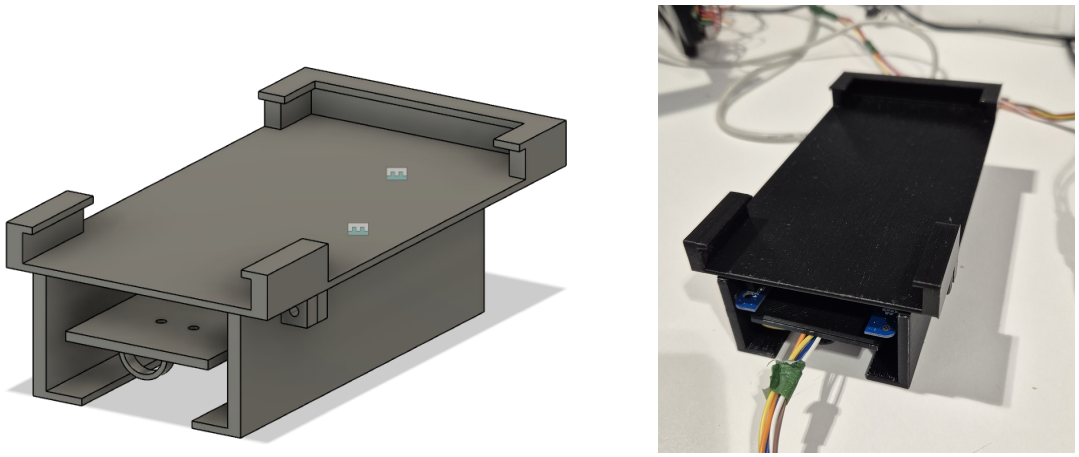

(a) 3D design of the phone holder

(b) 3D printed phone holder

Figure 6.4: 3D Design and model of the Phone holder

6.3. NFC evaluation

In this section, we evaluate and analyse the NFC connection with multiple experiments.

6.3.1. Buffer length

In the first experiment for the NFC link, we investigate how changing the message length affects the data rate of the NFC connection. We evaluate this by gradually increasing the amount of data that is sent per NFC message, ranging from 10 bytes to 250 bytes. To ensure the mailbox remains consistently filled, we send a new packet immediately after a previous one is successfully received by the phone and the GPO pin is triggered. During a timeframe of 10 seconds, the bps is calculated based on the total data received within that period. The results of this experiment are illustrated in figure 6.5.

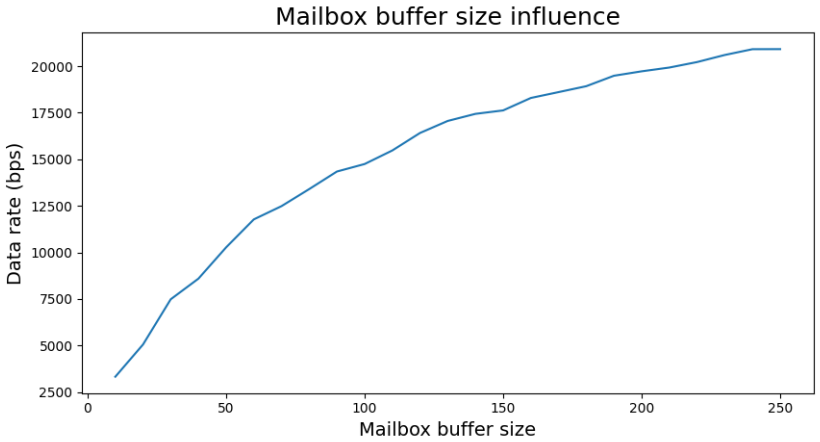

Figure 6.5: Buffer length experiment results

The results indicate that the data rate initially increases significantly when the mailbox buffer size until it is eventually maximized at 21000 bps. The initial large increments in data rate are likely due to the overhead associated with the I2C communication for writing data into the mailbox and the time taken by the phone to read the data from the mailbox.

Based on the findings of this experiment, the mailbox should always be filled to its maximum capacity. Therefore, we implemented a new functionality in which the MCU buffers the data that has to be sent via VLC. If the data length is below 250 bytes, we store the data in the buffer without sending it to the phone. Only when the buffer exceeds 250 bytes, we transmit the data to the phone via NFC. Any remaining data is buffered for the next NFC transmission phase.

6.3.2. Different phones

The second experiment analyzes the influence of different mobile phones on the NFC connection speed. This analysis aims to determine whether the performance characteristics of various phones could affect the throughput of the NFC communication. Four different mobile phones were tested: Samsung Galaxy S10e, Samsung Galaxy A34, Redmi Note 10, and Samsung Galaxy A34. The experimental results are presented in figure 6.6.

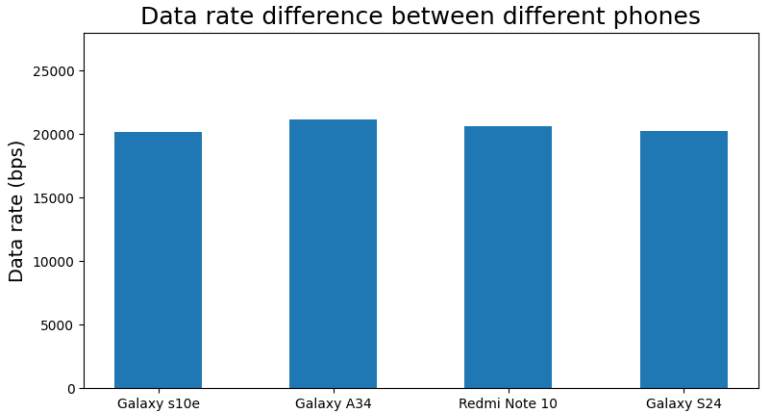

Figure 6.6: Experiment result showing the datarates of different phones

The results demonstrate no significant variation in the performance of the NFC system across the different phones tested. The data rate remains consistent regardless of the device, suggesting that the hardware or software does not impact the NFC communication.

7 Evaluation

In this section, we present the evaluation of the LightVest.

7.1. Number of decoding processes

With the LightVest, we have access to six individual photodiodes. So far, the sample that we use to demodulate the signal is taken from summing up all the ADC values from the photodiodes. The ADC samples are not taken at the same time. However, they are taken after each other. This may negatively impact the performance of the LightVest. The time difference between taking the first and last ADC sample is 2.997μs. This difference may be very small, but it is still important to explore other ways of demodulating the ADC samples. We can try to solve this by modulating every photodiode individually. However, this would result in more computational power.

In this experiment, we explore this with benchmarking tests to determine the maximum sampling rates and, with it, the amount of decoding processes. We do this using two key functions: one is about decoding a sample (explained in 5.6.3) and another for the ST25 tick (explained in 6.2.1), which checks for a GPO interrupt and performs a non-blocking I2C tick. The evaluation of various combinations can be seen in table 7.1.

Processes	time (μs)	Maximum sampling rate (kHz)
3 Decoding processes + ST25	6.5335	153.05
3 Decoding processes	5.496	181.95
2 Decoding processes + ST25	4.6846	213.67
1 Decoding process + ST25	2.8436	352
1 Decoding process	1.8536	540.54
ST25	0.96	1041.67

Table 7.1: Evaluation of various combinations of amount of process including and excluding the ST25

These results show that a sampling rate of 352 kHz can be reached when we only have one decoding process while sending the received VLC data to the phone with the ST25 tick. However, when we want to have three decoding processes and an ST25 tick, we can only achieve a maximum sampling rate of 153 kHz, more than half compared to only one decoding process. Ideally, we want to decode each photodiode individually. Based on this, handling six processes would require 12.06 μs, resulting in a sampling rate of 82 kHz, assuming everything else runs perfectly. This can be a problem when one, for example, wants to achieve a data rate of 20 kbps. With only having 8 samples per symbol (with Manchester encoding), the performance can be inadequate. Future work should analyse how much influence the amount of samples per period has on the data rate.

7.2. Movement

In this experiment, we analyse the performance of the LightVest during different types of movement. The LightVest should maintain a reliable data rate while the wearer is in motion. Three different movements are tested: static, walking, and running. For each movement, three data rates are evaluated: 5, 10, and 15 kbps.

We place the transmitter at a two-meter height and point it downwards. For static movement, the user stands close to the transmitter to gather the results in the most optimal setting. A three-meter path was used for the walking and running movements, with the transmitter positioned at the centre. The user always moves forward, and if it reaches the end of the path, he/she has to turn around and go back. A picture of how the experiment is set up can be seen in figure 7.1. For each experiment, the amount of data that has been received is recorded over 20 seconds and repeated 10 times to obtain an average value.

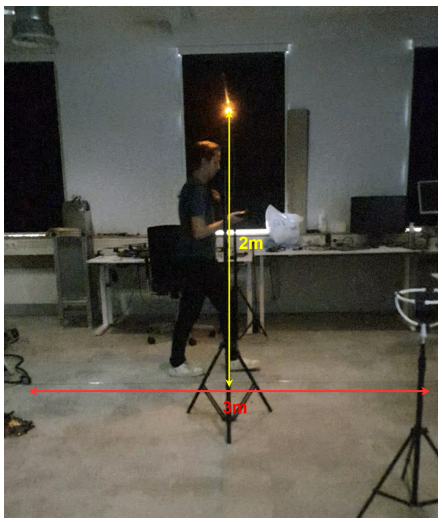

Figure 7.1: Visualization of how the experiment is set up

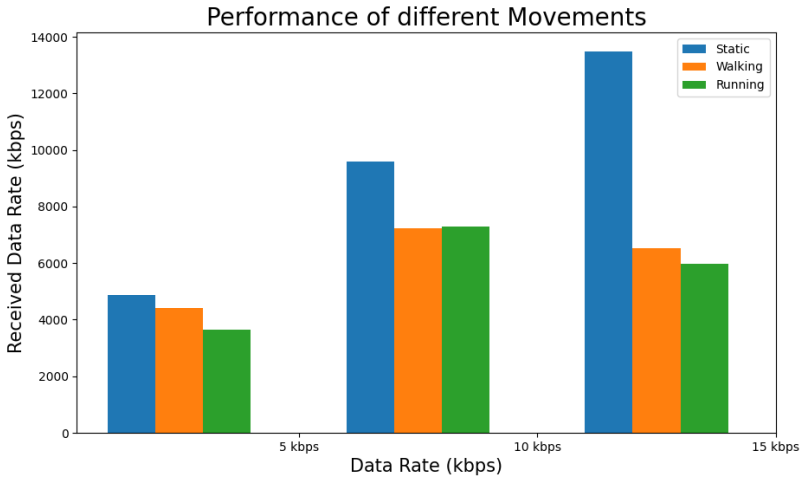

Figure 7.2: Result of the movement experiments

The results that can be seen in figure 7.2 show that static scenario consistently obtains the highest data rates compared to walking or running. For the 5kbps and 15kbps, walking resulted in a lower performance compared to the static movement, and running performed even worse.

This decline likely occurs due to the degraded signal reception when the user reaches the edges of the

3-meter path, leading to lost packets. We can confirm this reason because the higher the data rate, the larger the difference in received data rate is between static and walking. This hypothesis is supported by the observation that the performance gap between static and walking increases at higher data rates. A previous experiment in section 5.7.1 confirmed that having a higher data rate reduces its range.

7.3. Power consumption

This section evaluates the power consumption of the LightVest. Power efficiency is crucial within a wearable system since it relies on batteries. Lower power consumption allows for smaller batteries or extended operational time between charges.

First, power consumption is estimated based on datasheet specifications, followed by actual measurements to verify these estimates. LightVest has three primary power-consuming components: the MCU, photodiodes, and the NFC tag. The MCU draws power for computations, the photodiodes for their amplifier modules, and the ST25 draws power during active I2C communication. The power consumptions of the components are listed in table 7.2.

Component	Operation	Current
MCU	Normal operation	65 mA
	ADC	1.6 mA (Per ADC)
	HSE	530 μA
	Sleeping mode	10.2 mA
Photodiodes	Quiescent current	220 μA (per PD)
ST25	I2C read/write	220 μA
	I2C standby	76 μA
	I2C Power down	1.3 μA

Table 7.2: Power consumption based on the datasheets

Based on these values, the worst-case power consumption is estimated to be 70.27 mA, assuming the MCU operates normally (65 mA), six photodiodes are utilized (1.32 mA), and the I2C is continuously in operation (220 μA). However, this level of consumption is not always the same. When the LightVest is not receiving any VLC signals, the computational demand decreases, and the I2C interface remains inactive, resulting in reduced power consumption.

To assess the power consumption, we monitored the current draw in different operational modes using a power supply. The results are shown in table 7.3.

Operation	Current (mA)
Static	66–77
Transferring data over NFC	71-82
Vest experiment without light	71-82
Vest experiment with light	84

Table 7.3: Experimental current draw in various operations

These results suggest that, under typical operating conditions, the power consumption is higher than the datasheet estimates.

Implementing software features to detect when no VLC signal is received could reduce power consumption. This could allow the MCU to enter sleep mode, reducing the current draw to approximately 15.27 mA or even lower.

7.4. LightVest vs singular photodiode

In this experiment, we want to evaluate the differences between having one photodiode and LightVest. Singular photodiodes may experience performance degradation if they are obstructed by the user's body or if they are positioned at angles relative to the transmitter that are too steep. LightVest should

not face these problems. To address this, we evaluate the performance of LightVest by comparing BER values when using LightVest versus individual photodiodes under various orientations and locations.

The experiment is operated by placing LightVest at nine different locations. At each location, we measure the BER for each photodiode and LightVest within a timeframe of 10 seconds. The vest is then rotated by 90 degrees, preparing the BER measurements. This is done until the vest returns to its original orientation. Figure 7.3 illustrates the experimental setup and provides a photograph of the actual setup.

The hypothesis for this experiment is that LightVest will always provide better performance compared to a single photodiode. Especially when some photodiodes are unable to receive data due to their angle towards the transmitter or blockage.

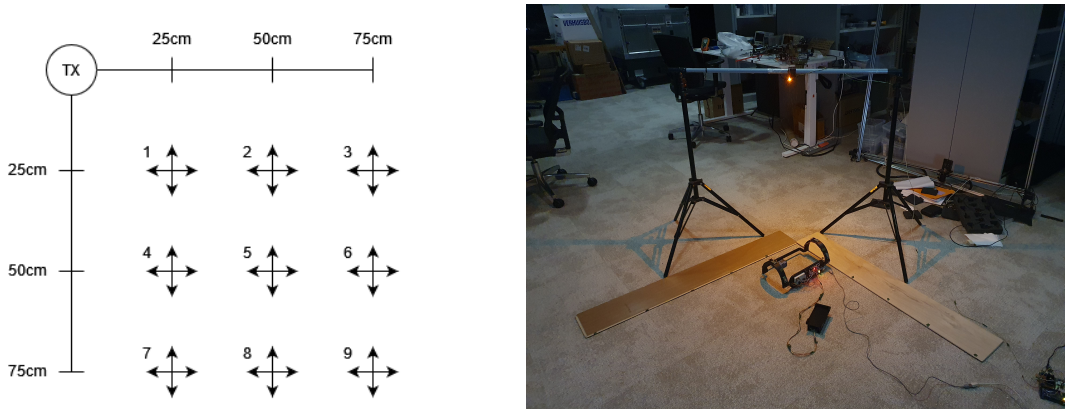

(a) Experiment map

(b) Photo of the experiment

Figure 7.3: LightVest 3D design

The experiment results, shown in figure 7.4, present a box plot for each location representing the BER values of all the individual photodiodes. The blue line represents the BER values of LightVest. To ensure readability, a BER of 0 was recorded as 0.0001.

In the results shown in figure 7.4 we can see that in the first location, all the individual photodiodes are able to receive the data correctly, having a BER of 0. However, in the other locations, the performance of individual photodiodes deteriorated. With some photodiodes even showing a BER greater than 10^{-3}. Despite this, there are always one or two photodiodes with a BER of 0. The blue line, representing the LightVest, follows the trend of the best-performing PD and even outperforms it at location 9, achieving a BER of 5.4×10^{-4} compared to the best PD achieving a BER of 2.9×10^{-3}. From this experiment, we can see that LightVest clearly outperforms singular photodiodes.

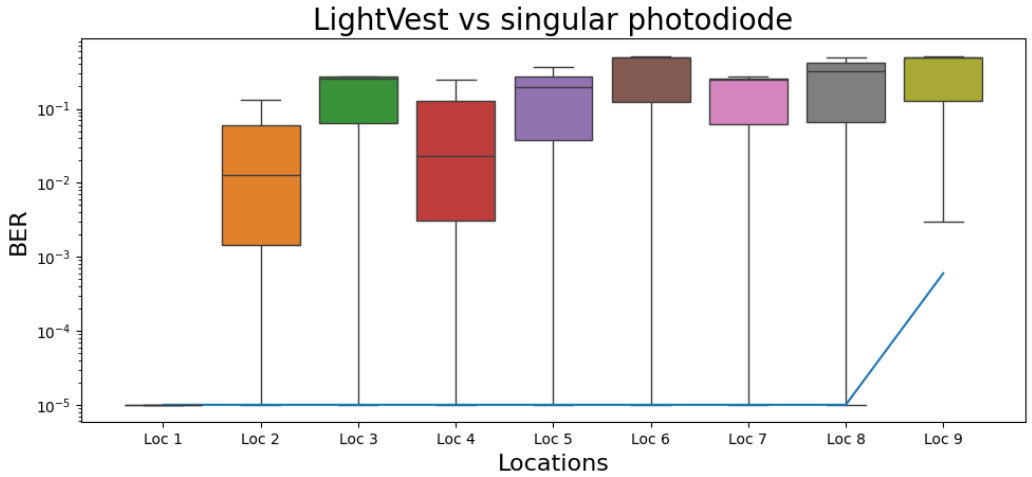

Figure 7.4: Results of the LightVest vs singular photodiode experiment

8

Conclusion

8.1. Conclusion

In this thesis, we presented the development and implementation of LightVest, a novel solution designed to address the extreme problem of Non-Line-of-Sight in Visible Light Communication when the receiver (such as a phone) is placed in a pocket, unable to receive VLC signals.

LightVest ensures this by utilizing photodiodes placed on a 3D-printed "vest". The processing unit demodulates and decodes the signals from the photodiodes and transfers the data to a dynamic NFC tag, which can connect and transmit the data to the phone. The implementation consists of two main components: the VLC link and the NFC link.

In the VLC link, we optimized the performance after multiple contributions. We conducted a study focusing on the placement and angles of the photodiodes on the vest. Using the Lambertian propagation model, we calculated the received power based on the angle between the transmitter and the receiver. A simulation and an experiment were set up, and we determined that an angle of 60 degrees was most effective. Next, we explored and evaluated the system when some movement is involved. With a filter and an adaptive threshold, we optimized the link performance. Additionally, we modified the software by enabling Direct Memory Access (DMA) to achieve a higher sampling rate. By carrying out a benchmark, we identified and resolved a bottleneck, speeding up processing a sample by 6.59 times. We evaluated the VLC link with an experiment to determine the maximum data rate and range, with the maximum data rate being 25 kbps and a range of 220 cm with a data rate of 5 kbps and a BER of 0.025.

In the NFC link, we explained the implementation with features like Fast Transfer Mode and non-blocking I2C. We enabled NFC communication by developing an Android app. The app also provides a menu option to control the MCU for debugging tools or experiment selection, which greatly sped up the debugging and experimentation process. We evaluated the NFC link with two experiments. The first experiment investigated the buffer length, which refers to the amount of data transferred during one transaction. The result shows that the buffer needs to be loaded to its full capacity to achieve the highest data rate of 21 kbps. In the other experiment, we analysed the influence of different mobile phones on the data rate, showing our system works well on all phones.

In the final chapter, we presented LightVest's evaluations. For the first evaluation, we performed a benchmark to determine the number of decoding processes the MCU can simultaneously run. The results showed that a sampling rate of 82 kHz is achievable when we want to have a demodulation process for every PD. In the second experiment, we assessed LightVest's performance during different types of movement, including static, walking, and running, at three different data rates: 5, 10, and 15 kbps. The results indicate that performance degrades for the walking and running movements, possibly due to poor reception at the path edges. To measure power consumption, we first looked at the datasheets and then measured the power consumption of the LightVest. According to the datasheets, LightVest should consume 70.27 mA when the MCU is active. However, the result was higher when we measured it, with a value of 84 mA. In the last experiment, we evaluated the differences in performance

between LightVest and singular photodiodes by comparing BER values under various orientations and locations. The results showed that LightVest is almost not affected when some photodiodes are blocked because it even outperforms the best singular photodiode in the last location.

8.2. Future work

In this thesis, we have presented the first prototype that combines VLC and NFC to provide VLC data to a mobile phone located inside a pocket. Further development could lead to a more sophisticated design or higher performance in several areas.

8.2.1. Vest design

Currently, we have used a 3D-printed model that poses as a "vest" to have a wearable design. Future work could explore alternative designs, such as integrating photodiodes into a shirt instead of a 3D-printed model.

8.2.2. Higher performance VLC link

The current VLC Link achieved a maximum data rate of 25 kbps by optimizing it with a filter and adaptive threshold, and we increased the sample rate with DMA by optimizing the software. However, several measures can be taken to further improve the VLC link's performance.

More powerful MCU

During the thesis, we chose the STM32F446RET because it passed all the requirements. However, other microprocessors were not considered. At this moment, we have achieved a maximum sampling rate of 352 kHz. A more powerful processing unit is required to achieve a higher sampling rate and, thus, higher data rate. There are multiple microprocessors available with higher maximum clock speeds that could be considered:

1. **STM32H7 series:** Featuring a dual-core processor and a clock speed of up to 600 MHz.
2. **Microchip Sam e70:** Offering a maximum clock speed of 300 MHz.
3. **NXP MX RT1060:** Offering a maximum clock speed of 600 MHz.

However, the consequence of having a higher-performance MCU might be an increase in power consumption, which should be taken into account.

Alternatively, an FPGA can be utilized, as the software and hardware are relatively straightforward. However, FPGAs can be quite expensive and may have high power consumption,

Enhanced filtering

This thesis used a simple filter to process the VLC signals. Implementing more advanced filtering techniques, such as Finite Impulse Response (FIR) or Infinite Impulse Response (IIR) filters, could enhance the precision of the signal processing and improve the overall performance of the VLC link. It can also be a cause for more processing power, which influences the sampling rate.

More advanced modulation

As for our modulation scheme, OOK with Manchester encoding is implemented in this thesis. This is a relatively simple modulation technique with a low spectral efficiency. A more advanced modulation such as FSK or PSK could be applied to further increase the data rate.

8.2.3. More evaluations

Additional evaluations could provide a deeper understanding of the system's capabilities and limitations. Unfortunately, due to time constraints, several experiments were not conducted.

Future work could include testing the system with users in various stances and environments with multiple light sources to evaluate the LightVest in a bigger area.

To fully test the implementation in realistic environments, such as offices or warehouses, brighter light sources can be used to more accurately simulate the system being used in its useful environments.

8.2.4. Uplink

In the thesis, we solely focused on the downlink from the transmitter to the receiver. For a complete VLC system, an uplink is necessary. Future work could involve the development of an uplink using infrared transmitters placed on the shoulders of the vest, with corresponding receivers located on the transmitter's side. This would enable a two-way communication system, enhancing the functionality of LightVest.

Bibliography

[1] Trio Adiono et al. "Visible light communication system for wearable patient monitoring device". In: *2016 IEEE Region 10 Conference (TENCON)*. Singapore: IEEE, Nov. 2016, pp. 1969–1972. ISBN: 978-1-5090-2597-8. DOI: 10.1109/TENCON.2016.7848367. URL: http://ieeexplore.ieee.org/document/7848367/ (visited on 12/15/2023).

[2] Amna Aliaberi, Paschalis C. Sofotasios, and Sami Muhaidat. "Modulation Schemes for Visible Light Communications". In: *2019 International Conference on Advanced Communication Technologies and Networking (CommNet)*. Rabat, Morocco: IEEE, Apr. 2019, pp. 1–10. ISBN: 978-1-5386-8317-0. DOI: 10.1109/COMMNET.2019.8742376. URL: https://ieeexplore.ieee.org/document/8742376/ (visited on 08/01/2024).

[3] Santanu Kumar Behera. "Chipless RFID Sensors for Wearable Applications: A Review". In: *IEEE Sensors Journal* 22.2 (Jan. 2022), pp. 1105–1120. ISSN: 1530-437X, 1558-1748, 2379-9153. DOI: 10.1109/JSEN.2021.3126487. URL: https://ieeexplore.ieee.org/document/9606752/ (visited on 02/22/2024).

[4] Jona Beysens, Qing Wang, and Sofie Pollin. "Exploiting Blockage in VLC Networks Through User Rotations". In: *IEEE Open Journal of the Communications Society* 1 (2020), pp. 1084–1099. ISSN: 2644-125X. DOI: 10.1109/OJCOMS.2020.3010021. URL: https://ieeexplore.ieee.org/document/9143202/ (visited on 12/15/2023).

[5] Jona Beysens, Qing Wang, and Sofie Pollin. "Improving Blockage Robustness in VLC Networks". In: *2019 11th International Conference on Communication Systems & Networks (COMSNETS)*. Bengaluru, India: IEEE, Jan. 2019, pp. 164–171. ISBN: 978-1-5386-7902-9. DOI: 10.1109/COMSNETS.2019.8711037. URL: https://ieeexplore.ieee.org/document/8711037/ (visited on 01/16/2024).

[6] Alin-Mihai Căilean et al. "Visible Light Communications-Based Assistance System for the Blind and Visually Impaired: Design, Implementation, and Intensive Experimental Evaluation in a Real-Life Situation". en. In: *Sensors* 23.23 (Nov. 2023), p. 9406. ISSN: 1424-8220. DOI: 10.3390/s23239406. URL: https://www.mdpi.com/1424-8220/23/23/9406 (visited on 03/07/2024).

[7] Chi-Wai Chow et al. "Using advertisement light-panel and CMOS image sensor with frequency-shift-keying for visible light communication". en. In: *Optics Express* 26.10 (May 2018), p. 12530. ISSN: 1094-4087. DOI: 10.1364/OE.26.012530. URL: https://opg.optica.org/abstract.cfm?URI=oe-26-10-12530 (visited on 07/16/2024).

[8] Mostafa Zaman Chowdhury et al. "A Comparative Survey of Optical Wireless Technologies: Architectures and Applications". In: *IEEE Access* 6 (2018), pp. 9819–9840. ISSN: 2169-3536. DOI: 10.1109/ACCESS.2018.2792419. URL: http://ieeexplore.ieee.org/document/8259465/ (visited on 07/15/2024).

[9] Jiska Classen et al. "The Spy Next Door: Eavesdropping on High Throughput Visible Light Communications". en. In: *Proceedings of the 2nd International Workshop on Visible Light Communications Systems*. Paris France: ACM, Sept. 2015, pp. 9–14. ISBN: 978-1-4503-3702-1. DOI: 10.1145/2801073.2801075. URL: https://dl.acm.org/doi/10.1145/2801073.2801075 (visited on 01/25/2024).

[10] Minhao Cui, Qing Wang, and Jie Xiong. "Bracelet+: Harvesting the Leaked RF Energy in VLC with Wearable Bracelet Antenna". en. In: *Proceedings of the 20th ACM Conference on Embedded Networked Sensor Systems*. Boston Massachusetts: ACM, Nov. 2022, pp. 250–262. ISBN: 978-1-4503-9886-2. DOI: 10.1145/3560905.3568526. URL: https://dl.acm.org/doi/10.1145/3560905.3568526 (visited on 08/02/2024).

[11] Minhao Cui, Qing Wang, and Jie Xiong. "Breaking the limitations of visible light communication through its side channel". en. In: *Proceedings of the 18th Conference on Embedded Networked Sensor Systems*. Virtual Event Japan: ACM, Nov. 2020, pp. 232–244. ISBN: 978-1-4503-7590-0. DOI: 10.1145/3384419.3430728. URL: https://dl.acm.org/doi/10.1145/3384419.3430728 (visited on 12/15/2023).

[12] James Davis, Yi-Hsuan Hsieh, and Hung-Chi Lee. "Humans perceive flicker artifacts at 500 Hz". en. In: *Scientific Reports* 5.1 (Feb. 2015), p. 7861. ISSN: 2045-2322. DOI: 10.1038/srep07861. URL: https://www.nature.com/articles/srep07861 (visited on 08/27/2024).

[13] Valeria Galli et al. "Passive and Wireless All-Textile Wearable Sensor System". en. In: *Advanced Science* 10.22 (Aug. 2023), p. 2206665. ISSN: 2198-3844, 2198-3844. DOI: 10.1002/advs.202206665. URL: https://onlinelibrary.wiley.com/doi/10.1002/advs.202206665 (visited on 02/20/2024).

[14] Baptiste Garnier et al. "Analysis of the power transfer and electrical performances of an embroidered textile loop antenna for near field communication (NFC) application". In: *IOP Conference Series: Materials Science and Engineering* 827.1 (Apr. 2020), p. 012030. ISSN: 1757-8981, 1757-899X. DOI: 10.1088/1757-899X/827/1/012030. URL: https://iopscience.iop.org/article/10.1088/1757-899X/827/1/012030 (visited on 02/22/2024).

[15] Baptiste Garnier et al. "Electronic-components less fully textile multiple resonant combiners for body-centric near field communication". en. In: *Scientific Reports* 11.1 (Jan. 2021), p. 2159. ISSN: 2045-2322. DOI: 10.1038/s41598-021-81246-z. URL: https://www.nature.com/articles/s41598-021-81246-z (visited on 03/26/2024).

[16] Seyed Keyarash Ghiasi, Marco A. Zúñiga Zamalloa, and Koen Langendoen. "A principled design for passive light communication". en. In: *Proceedings of the 27th Annual International Conference on Mobile Computing and Networking*. New Orleans Louisiana: ACM, Sept. 2021, pp. 121–133. ISBN: 978-1-4503-8342-4. DOI: 10.1145/3447993.3448629. URL: https://dl.acm.org/doi/10.1145/3447993.3448629 (visited on 07/04/2024).

[17] Domenico Giustiniano, Nils Ole Tippenhauer, and Stefan Mangold. "Low-complexity Visible Light Networking with LED-to-LED communication". In: *2012 IFIP Wireless Days*. Dublin, Ireland: IEEE, Nov. 2012, pp. 1–8. ISBN: 978-1-4673-4404-3 978-1-4673-4402-9 978-1-4673-4403-6. DOI: 10.1109/WD.2012.6402861. URL: http://ieeexplore.ieee.org/document/6402861/ (visited on 07/04/2024).

[18] Liane Grobe et al. "High-speed visible light communication systems". In: *IEEE Communications Magazine* 51.12 (Dec. 2013), pp. 60–66. ISSN: 0163-6804. DOI: 10.1109/MCOM.2013.6685758. URL: https://ieeexplore.ieee.org/document/6685758/ (visited on 01/12/2024).

[19] Hooman Hematkhah and Yousef Seifi Kavian. "Performance Evaluation of Polar Channel Coding on a Practical VLC Link: A Comparison Study". In: *2020 3rd West Asian Symposium on Optical and Millimeter-wave Wireless Communication (WASOWC)*. Tehran, Iran: IEEE, Nov. 2020, pp. 1–6. ISBN: 978-1-72818-691-7. DOI: 10.1109/WASOWC49739.2020.9410037. URL: https://ieeexplore.ieee.org/document/9410037/ (visited on 07/16/2024).

[20] Honglei Li Honglei Li et al. "High-speed phosphorescent white LED visible light communications without utilizing a blue filter". en. In: *Chinese Optics Letters* 13.8 (2015), pp. 080605–80609. ISSN: 1671-7694. DOI: 10.3788/COL201513.080605. URL: https://www.researching.cn/articles/OJ54cbaae3cbefc564/html (visited on 08/02/2024).

[21] Texas Instruments. *OPT101 Datasheet*. Oct. 2003.

[22] J.M. Kahn and J.R. Barry. "Wireless infrared communications". In: *Proceedings of the IEEE* 85.2 (Feb. 1997), pp. 265–298. ISSN: 00189219. DOI: 10.1109/5.554222. URL: http://ieeexplore.ieee.org/document/554222/ (visited on 02/06/2024).

[23] Tianxing Li et al. "Real-Time Screen-Camera Communication Behind Any Scene". en. In: *Proceedings of the 13th Annual International Conference on Mobile Systems, Applications, and Services*. Florence Italy: ACM, May 2015, pp. 197–211. ISBN: 978-1-4503-3494-5. DOI: 10.1145/2742647.2742667. URL: https://dl.acm.org/doi/10.1145/2742647.2742667 (visited on 07/04/2024).

[24] Xiaohan Liu et al. "Design of an Indoor Self-Positioning System for the Visually Impaired - Simulation with RFID and Bluetooth in a Visible Light Communication System". In: *2007 29th Annual International Conference of the IEEE Engineering in Medicine and Biology Society*. ISSN: 1557-170X. Lyon, France: IEEE, Aug. 2007, pp. 1655–1658. ISBN: 978-1-4244-0787-3 978-1-4244-0788-0. DOI: 10.1109/IEMBS.2007.4352625. URL: http://ieeexplore.ieee.org/document/4352625/ (visited on 07/17/2024).

[25] Bilal Malik and Xun Zhang. "Solar panel receiver system implementation for visible light communication". In: *2015 IEEE International Conference on Electronics, Circuits, and Systems (ICECS)*. Cairo: IEEE, Dec. 2015, pp. 502–503. ISBN: 978-1-5090-0246-7. DOI: 10.1109/ICECS.2015.7440361. URL: http://ieeexplore.ieee.org/document/7440361/ (visited on 07/15/2024).

[26] Luiz Eduardo Mendes Matheus et al. "Visible Light Communication: Concepts, Applications and Challenges". In: *IEEE Communications Surveys & Tutorials* 21.4 (2019). Conference Name: IEEE Communications Surveys & Tutorials, pp. 3204–3237. ISSN: 1553-877X. DOI: 10.1109/COMST.2019.2913348. URL: https://ieeexplore.ieee.org/abstract/document/8698841?casa_token=qPeubUN2RfkAAAAA:YcXiG0lwIS49LHZw1_xuarRJwHF3uVlKzJexKir5TSt2E_G8PmnA-Cg4goSFJoUiUwt8l6k (visited on 11/20/2023).

[27] Eric Monteiro and Steve Hranilovic. "Design and Implementation of Color-Shift Keying for Visible Light Communications". In: *Journal of Lightwave Technology* 32.10 (May 2014), pp. 2053–2060. ISSN: 0733-8724, 1558-2213. DOI: 10.1109/JLT.2014.2314358. URL: http://ieeexplore.ieee.org/document/6780585/ (visited on 08/02/2024).

[28] Volkan Rodoplu et al. "Characterization of Line-of-Sight Link Availability in Indoor Visible Light Communication Networks Based on the Behavior of Human Users". In: *IEEE Access* 8 (2020), pp. 39336–39348. ISSN: 2169-3536. DOI: 10.1109/ACCESS.2020.2974704. URL: https://ieeexplore.ieee.org/document/9000876/ (visited on 01/24/2024).

[29] Anand Singh et al. "Performance Analysis of Indoor Communication System Using Off-the-Shelf LEDs With Human Blockages". In: *IEEE Open Journal of the Communications Society* 2 (2021), pp. 187–198. ISSN: 2644-125X. DOI: 10.1109/OJCOMS.2020.3048954. URL: https://ieeexplore.ieee.org/document/9314907/ (visited on 01/25/2024).

[30] STMicroelectronics. *STM32F446xC/E*. Jan. 2021.

[31] STMicroelectronics. *X-NUCLEO-NFC07A1 Data brief*.

[32] Elise Talgorn and Helle Ullerup. "Invoking 'Empathy for the Planet' through Participatory Ecological Storytelling: From Human-Centered to Planet-Centered Design". en. In: *Sustainability* 15.10 (May 2023), p. 7794. ISSN: 2071-1050. DOI: 10.3390/su15107794. URL: https://www.mdpi.com/2071-1050/15/10/7794 (visited on 08/22/2024).

[33] Stefan Videv and Harald Haas. "Practical space shift keying VLC system". In: *2014 IEEE Wireless Communications and Networking Conference (WCNC)*. Istanbul, Turkey: IEEE, Apr. 2014, pp. 405–409. ISBN: 978-1-4799-3083-8. DOI: 10.1109/WCNC.2014.6952042. URL: http://ieeexplore.ieee.org/document/6952042/ (visited on 07/17/2024).

[34] Ge Wang et al. "Cross-technology Communication between Visible Light and Battery-free RFIDs". en. In: *Proceedings of the ACM on Interactive, Mobile, Wearable and Ubiquitous Technologies* 7.3 (Sept. 2023), pp. 1–20. ISSN: 2474-9567. DOI: 10.1145/3610883. URL: https://dl.acm.org/doi/10.1145/3610883 (visited on 03/07/2024).

[35] Qing Wang and Domenico Giustiniano. "Intra-Frame Bidirectional Transmission in Networks of Visible LEDs". In: *IEEE/ACM Transactions on Networking* 24.6 (Dec. 2016), pp. 3607–3619. ISSN: 1063-6692, 1558-2566. DOI: 10.1109/TNET.2016.2530874. URL: http://ieeexplore.ieee.org/document/7423788/ (visited on 02/05/2024).

[36] Qing Wang, Marco Zuniga, and Domenico Giustiniano. "Passive Communication with Ambient Light". en. In: *Proceedings of the 12th International on Conference on emerging Networking EXperiments and Technologies*. Irvine California USA: ACM, Dec. 2016, pp. 97–104. ISBN: 978-1-4503-4292-6. DOI: 10.1145/2999572.2999584. URL: https://dl.acm.org/doi/10.1145/2999572.2999584 (visited on 07/04/2024).

[37] Zhaocheng Wang, Tianqi Mao, and Qi Wang. "Optical OFDM for visible light communications". In: *2017 13th International Wireless Communications and Mobile Computing Conference (IWCMC)*. Valencia, Spain: IEEE, June 2017, pp. 1190–1194. ISBN: 978-1-5090-4372-9. DOI: 10.1109/IWCMC.2017.7986454. URL: http://ieeexplore.ieee.org/document/7986454/ (visited on 08/02/2024).

[38] Hongjia Wu et al. "SmartVLC: Co-Designing Smart Lighting and Communication for Visible Light Networks". In: *IEEE Transactions on Mobile Computing* 19.8 (Aug. 2020), pp. 1956–1970. ISSN: 1536-1233, 1558-0660, 2161-9875. DOI: 10.1109/TMC.2019.2915220. URL: https://ieeexplore.ieee.org/document/8708935/ (visited on 02/05/2024).

[39] Lulu Xu et al. "Deformation-Resilient Embroidered Near Field Communication Antenna and Energy Harvesters for Wearable Applications". en. In: *Advanced Intelligent Systems* 1.6 (Oct. 2019), p. 1900056. ISSN: 2640-4567, 2640-4567. DOI: 10.1002/aisy.201900056. URL: https://onlinelibrary.wiley.com/doi/10.1002/aisy.201900056 (visited on 03/26/2024).

[40] Yanbing Yang and Jun Luo. "Boosting the Throughput of LED-Camera VLC via Composite Light Emission". In: *IEEE INFOCOM 2018 - IEEE Conference on Computer Communications*. Honolulu, HI:

IEEE, Apr. 2018, pp. 315–323. ISBN: 978-1-5386-4128-6. DOI: 10.1109/INFOCOM.2018.8486209. URL: https://ieeexplore.ieee.org/document/8486209/ (visited on 07/16/2024).

[41] Yanbing Yang, Jiangtian Nie, and Jun Luo. "ReflexCode: Coding with Superposed Reflection Light for LED-Camera Communication". en. In: *Proceedings of the 23rd Annual International Conference on Mobile Computing and Networking*. Snowbird Utah USA: ACM, Oct. 2017, pp. 193–205. ISBN: 978-1-4503-4916-1. DOI: 10.1145/3117811.3117836. URL: https://dl.acm.org/doi/10.1145/3117811.3117836 (visited on 07/16/2024).

[42] Yanbing Yang et al. "Pushing the Data Rate of Practical VLC via Combinatorial Light Emission". In: *IEEE Transactions on Mobile Computing* 20.5 (May 2021), pp. 1979–1992. ISSN: 1536-1233, 1558-0660, 2161-9875. DOI: 10.1109/TMC.2020.2971204. URL: https://ieeexplore.ieee.org/document/8978742/ (visited on 02/05/2024).

A

Filter and adaptive threshold parameter Experiment

In this experiment, optimal values for the filter and the adaptive threshold are determined. The transmitter is placed at a height of 110cm facing downwards. The receiver is placed on the ground, and placed at distances of 25, 50 and 75 cm. By increasing the α value from 10 to 60 with steps of 5 and the adaptive threshold value β (which is explained in the next section) from 0.005 to 0.1 with steps of 0.005 the best-performing combination of settings was determined. At each combination, the BER is calculated with a data rate of 5kbps, with a duration of 10 seconds. The result can be seen in the following figures. After reviewing the result, **a filter parameter of 45 and an adaptive threshold parameter of 0.015** are determined.

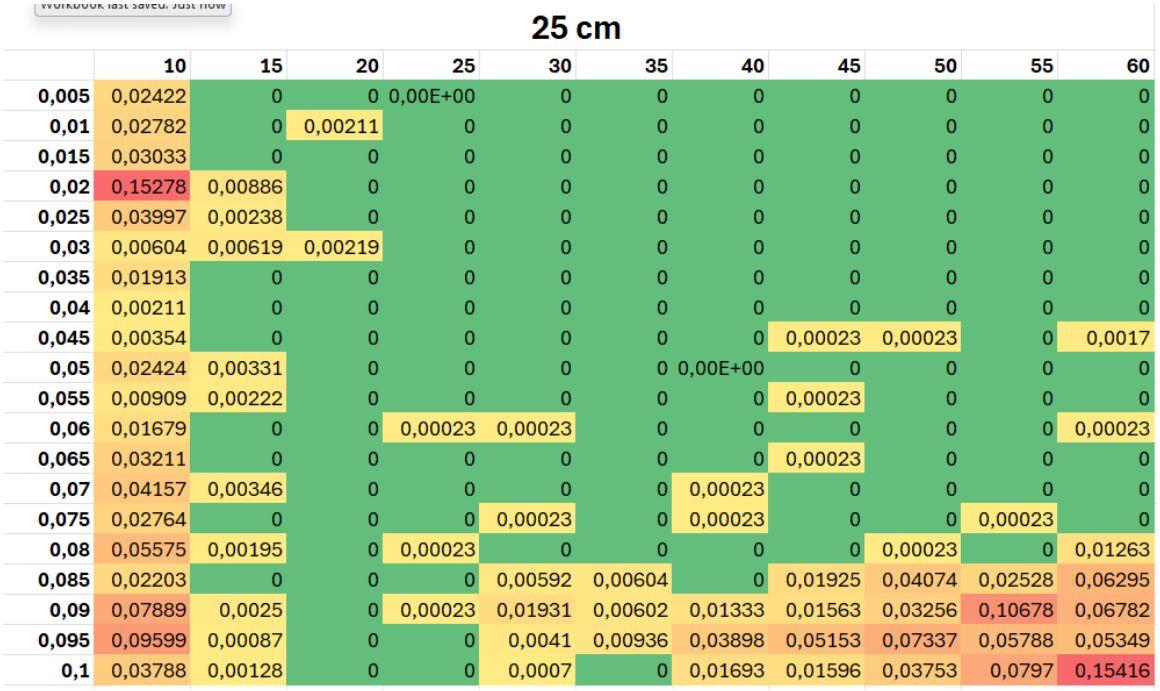

25 cm

	10	15	20	25	30	35	40	45	50	55	60
0,005	0,02422	0	0	0,00E+00	0	0	0	0	0	0	0
0,01	0,02782	0	0,00211	0	0	0	0	0	0	0	0
0,015	0,03033	0	0	0	0	0	0	0	0	0	0
0,02	0,15278	0,00886	0	0	0	0	0	0	0	0	0
0,025	0,03997	0,00238	0	0	0	0	0	0	0	0	0
0,03	0,00604	0,00619	0,00219	0	0	0	0	0	0	0	0
0,035	0,01913	0	0	0	0	0	0	0	0	0	0
0,04	0,00211	0	0	0	0	0	0	0	0	0	0
0,045	0,00354	0	0	0	0	0	0	0,00023	0,00023	0	0,0017
0,05	0,02424	0,00331	0	0	0	0	0,00E+00	0	0	0	0
0,055	0,00909	0,00222	0	0	0	0	0	0,00023	0	0	0
0,06	0,01679	0	0	0,00023	0,00023	0	0	0	0	0	0,00023
0,065	0,03211	0	0	0	0	0	0	0,00023	0	0	0
0,07	0,04157	0,00346	0	0	0	0	0,00023	0	0	0	0
0,075	0,02764	0	0	0	0,00023	0	0,00023	0	0	0,00023	0
0,08	0,05575	0,00195	0	0,00023	0	0	0	0	0,00023	0	0,01263
0,085	0,02203	0	0	0	0,00592	0,00604	0	0,01925	0,04074	0,02528	0,06295
0,09	0,07889	0,0025	0	0,00023	0,01931	0,00602	0,01333	0,01563	0,03256	0,10678	0,06782
0,095	0,09599	0,00087	0	0	0,0041	0,00936	0,03898	0,05153	0,07337	0,05788	0,05349
0,1	0,03788	0,00128	0	0	0,0007	0	0,01693	0,01596	0,03753	0,0797	0,15416

Figure A.1: Experiment results at a distance of 25 cm

50 cm

	10	15	20	25	30	35	40	45	50	55	60
0,005	1	1	0,36701	0,18107	0,06682	0,05434	0,02056	0,01281	0,01273	0,00041	0,0083
0,01	1	0,48512	0,23941	0,06092	0,01695	0,01294	0,01288	0,00874	0,00077	0,00224	0
0,015	1	0,39039	0,20712	0,0465	0,02424	0,01047	0,00068	0	0,00923	0,01199	0,03362
0,02	1	0,44131	0,19869	0,02906	0,01588	0,00869	0,02205	0,03664	0,02049	0,01867	0,01323
0,025	0,5514	0,09506	0,03403	0,00211	0,00311	0	0,02281	0,06049	0,10046	0,12566	0,17807
0,03	0,65066	0,3052	0,09777	0,06099	0,0503	0,08082	0,09152	0,20066	0,2764	0,32553	0,29738
0,035	0,29342	0,10951	0,03619	0,01246	0,04186	0,10516	0,14638	0,20757	0,14319	0,07426	0,25009
0,04	0,47452	0,22024	0,05604	0,05202	0,09059	0,19424	0,1729	0,2274	0,3317	0,4233	0,3572
0,045	0,56215	0,21732	0,05794	0,09305	0,11589	0,18958	0,24782	0,33313	0,39053	0,43475	0,48226
0,05	0,4515	0,12388	0,07363	0,09073	0,12793	0,15182	0,16648	0,2622	0,25699	0,35147	0,38198
0,055	0,35933	0,11193	0,04316	0,04474	0,12609	0,17435	0,22092	0,17437	0,27115	0,37387	0,32636
0,06	0,33234	0,11988	0,0862	0,12887	0,18045	0,23624	0,19542	0,31158	0,37014	0,34898	0,43193
0,065	0,27162	0,09162	0,04349	0,08109	0,05792	0,21225	0,30592	0,31369	0,41486	0,44688	0,45851
0,07	0,3548	0,08945	0,05277	0,08614	0,16309	0,22397	0,32946	0,278	0,33923	0,49383	0,51025
0,075	0,25713	0,0249	0,00625	0,00617	0,01221	0,03981	0,08875	0,20492	0,18842	0,30249	0,32151
0,08	0,20463	0,0359	0,00112	0,00023	0,03352	0,04492	0,118	0,12015	0,1908	0,25606	0,38794
0,085	0,1765	0,01687	0	0,00594	0,03488	0,09636	0,154	0,30437	0,42336	0,39985	0,46547
0,09	0,16097	0,01207	0,00317	0,05086	0,13325	0,20358	0,25788	0,34517	0,40703	0,44806	0,43796
0,095	0,08862	0,00549	0,0036	0,00898	0,01582	0,06084	0,10353	0,1192	0,16093	0,23682	0,29557
0,1	0,1457	0,03668	0,01755	0,06161	0,06747	0,17652	0,22107	0,2574	0,28102	0,41274	0,43788

Figure A.2: Experiment results at a distance of 50 cm

75 cm

	10	15	20	25	30	35	40	45	50	55	60
0,005	1	0,06186	0,00441	0,00E+00	0,00818	0	0,00193	0,00294	0	0	0
0,01	1	0,09974	0,01776	0,04774	0,03795	0,00629	0,00975	0,00041	0	0,00267	0
0,015	1	0,55709	0,18946	0,06297	0,02033	0,00801	0,00741	0	0	0,00035	0
0,02	1	0,46063	0,16975	0,02575	0,01325	0,00888	0,00085	0	0,00313	0	0,00248
0,025	1	0,38484	0,17712	0,05316	0,00936	0,00397	0,04426	0,04962	0,00588	0,00257	0,00594
0,03	0,64284	0,44131	0,19869	0,02906	0,01588	0,00869	0,02205	0,03664	0,02049	0,01867	0,01323
0,035	1	0,4386	0,28363	0,04138	0,01296	0,01008	0,0013	0	0	0,00751	0,00406
0,04	0,55215	0,20248	0,03803	0,00238	0,00091	0,00062	0	0	0	0	0,00226
0,045	0,57397	0,2946	0,07299	0,00472	0	-0,00195	0,30371	0,01575	0,53203	0	0,00958
0,05	0,58452	0,33441	0,06931	0,01211	0,02389	0,00294	0,0007	0,56635	1	0,08341	0,67905
0,055	1	1	1	1	0,47249	1	1	1	1	1	1
0,06	0,51942	1	1	1	1	1	1	0,02735	0,01221	0,09767	0,1582
0,065	0,59792	0,26901	0,03027	0,02623	0,00588	0,62851	0,03867	0,0454	0,05237	0,07612	0,09928
0,07	0,56622	0,26446	0,07651	0,01737	0,02933	0,10365	0,05912	0,08661	0,10024	0,33089	0,1536
0,075	0,60444	0,27963	0,61758	0,3801	1	1	1	1	1	1	0,69325
0,08	1	1	1	1	1	1	1	1	1	1	1
0,085	1	1	0,43216	1	1	1	1	1	1	1	1
0,09	1	1	1	1	1	1	1	1	1	1	1
0,095	1	1	1	1	1	1	0,54463	0,67184	0,66965	1	1
0,1	1	1	1	1	1	1	1	1	1	1	1

Figure A.3: Experiment results at a distance of 75 cm

Combined results

	10	15	20	25	30	35	40	45	50	55	60
0,005	0,67474	0,35395	0,12381	0,06036	0,025	0,01811	0,00749	0,00525	0,00424	0,00014	0,00277
0,01	0,67594	0,19495	0,08643	0,03622	0,0183	0,00641	0,00754	0,00305	0,00026	0,00164	0
0,015	0,67678	0,31583	0,13219	0,03649	0,01486	0,00616	0,0027	0	0,00308	0,00411	0,01121
0,02	0,71759	0,3036	0,12281	0,01827	0,00971	0,00586	0,00763	0,01221	0,00787	0,00622	0,00524
0,025	0,53046	0,16076	0,07038	0,01842	0,00415	0,00132	0,02236	0,0367	0,03545	0,04274	0,06134
0,03	0,43318	0,43713	0,36666	0,35366	0,3501	0,36027	0,36384	0,40022	0,28827	0,22928	0,43246
0,035	0,43752	0,1827	0,10661	0,01795	0,01827	0,03841	0,04923	0,06919	0,04773	0,02726	0,08472
0,04	0,34292	0,14091	0,03136	0,01813	0,0305	0,06495	0,05763	0,0758	0,11057	0,1411	0,11982
0,045	0,37988	0,17064	0,04365	0,03259	0,03863	0,06255	0,18384	0,11637	0,30759	0,14492	0,16451
0,05	0,35342	0,15387	0,04765	0,03428	0,05061	0,05159	0,05573	0,27618	0,419	0,14496	0,35368
0,055	0,45614	0,37138	0,34772	0,34825	0,19953	0,39145	0,40697	0,39153	0,42372	0,45796	0,44212
0,06	0,28952	0,37329	0,36207	0,37636	0,39356	0,41208	0,39847	0,11297	0,12745	0,14888	0,19679
0,065	0,30055	0,12021	0,02459	0,03577	0,02127	0,28026	0,11486	0,11977	0,15574	0,17433	0,18593
0,07	0,32086	0,11912	0,04309	0,0345	0,06414	0,10921	0,1296	0,12154	0,14649	0,27491	0,22128
0,075	0,2964	0,10151	0,20795	0,12876	0,33748	0,3466	0,36299	0,40164	0,39614	0,43424	0,33825
0,08	0,42013	0,34595	0,33371	0,33349	0,34451	0,34831	0,37267	0,37338	0,39701	0,41869	0,46686
0,085	0,39951	0,33896	0,14405	0,33531	0,34693	0,36747	0,38467	0,44121	0,48803	0,47504	0,50947
0,09	0,41329	0,33819	0,33439	0,35036	0,38419	0,4032	0,42374	0,4536	0,47986	0,51828	0,50193
0,095	0,39487	0,33545	0,33453	0,33633	0,33997	0,35673	0,22905	0,28086	0,30132	0,43157	0,44969
0,1	0,39453	0,34599	0,33918	0,35387	0,35606	0,39217	0,41267	0,42445	0,43952	0,49748	0,53068

Figure A.4: Experiment results at a distance all the combined results